AD-A073 954 STANFORD UNIV CA DEPT OF MECHANICAL ENGINEERING F/G 20/4
INSTRUMENTATION FOR THE MEASUREMENT OF TURBULENCE COMPONENTS IN--ETC(U)
AUG 79 M FROTA, R J MOFFAT AFOSR-78-3597
UNCLASSIFIED AFOSR-TR-79-0957

1 OF 1
AD
A073954

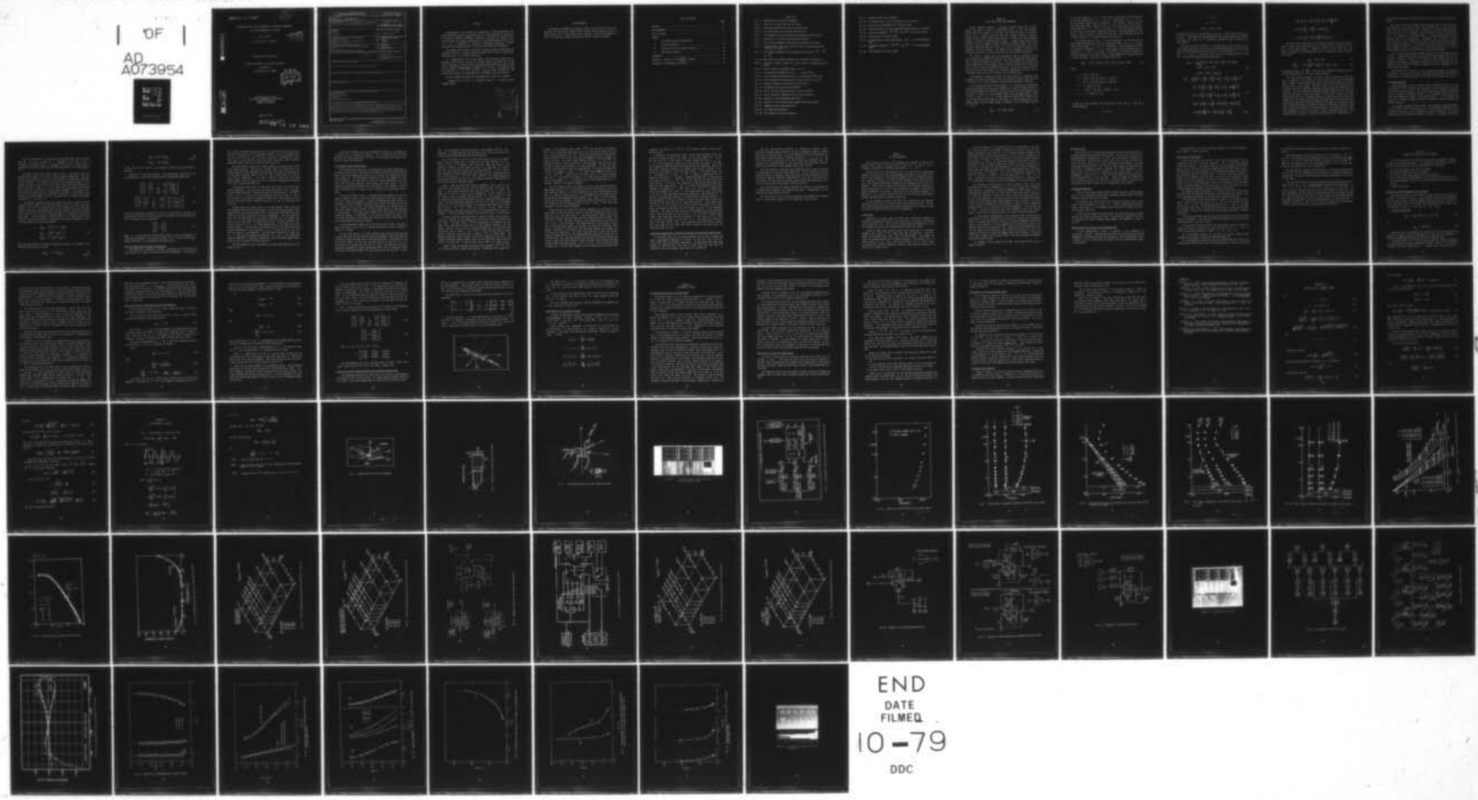

END
DATE
FILMED
10-79
DDC

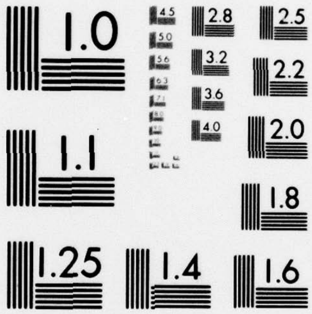
1.0
4.5
5.0
5.6
6.3
2.8
3.2
3.6
4.0
2.5
2.2
2.0
1.1
1.8
1.25
1.4
1.6

AFOSR-TR- 79-0957

12

INSTRUMENTATION FOR THE MEASUREMENT OF TURBULENCE COMPONENTS IN A THREE-DIMENSIONAL FLOW FIELD

LEVEL II

AFOSR 78-3597

M. Frota and R. J. Moffat

Prepared with Support from

The Air Force Office of Scientific Research
Building 410
Bolling AFB, D.C. 20332

DDC
RECEIVED
SEP 18 1979
A

Thermosciences Division
Department of Mechanical Engineering
Stanford University
Stanford, California

August 23, 1979

⑲ REPORT DOCUMENTATION PAGE

READ INSTRUCTIONS
BEFORE COMPLETING FORM

1. REPORT NUMBER ⑱ AFOSR-TR-79-0957	2. GOVT ACCESSION NO.	3. RECIPIENT'S CATALOG NUMBER
4. TITLE (and Subtitle) ⑥ INSTRUMENTATION FOR THE MEASUREMENT OF TURBULENCE COMPONENTS IN A THREE-DIMENSIONAL FLOW FIELD.		5. TYPE OF REPORT & PERIOD COVERED ⑨ FINAL rept. 1 May 1978 - 30 Nov 1978 6. PERFORMING ORG. REPORT NUMBER
7. AUTHOR(s) ⑩ M. FROTA R. J. MOFFAT	⑮	8. CONTRACT OR GRANT NUMBER(s) AFOSR-78-3597
9. PERFORMING ORGANIZATION NAME AND ADDRESS STANFORD UNIVERSITY DEPARTMENT OF MECHANICAL ENGINEERING STANFORD, CA 94305	⑯	10. PROGRAM ELEMENT, PROJECT, TASK AREA & WORK UNIT NUMBERS 2307A4 ⑰ A4 61102F
11. CONTROLLING OFFICE NAME AND ADDRESS AIR FORCE OFFICE OF SCIENTIFIC RESEARCH/NA BLDG 410 BOLLING AIR FORCE BASE, D C 20332	⑪	12. REPORT DATE Aug 79 13. NUMBER OF PAGES 75
14. MONITORING AGENCY NAME & ADDRESS(if different from Controlling Office) ⑫ 76p.		15. SECURITY CLASS. (of this report) UNCLASSIFIED 15a. DECLASSIFICATION/DOWNGRADING SCHEDULE

16. DISTRIBUTION STATEMENT (of this Report)

Approved for public release; distribution unlimited.

17. DISTRIBUTION STATEMENT (of the abstract entered in Block 20, if different from Report)

18. SUPPLEMENTARY NOTES

19. KEY WORDS (Continue on reverse side if necessary and identify by block number)

INSTRUMENTATION
HOT-WIRE ANEMOMETRY
TURBULENCE
THREE-DIMENSIONAL FLOW

20. ABSTRACT (Continue on reverse side if necessary and identify by block number)

A three-coordinate hot-wire anemometer system for turbulence measurements has been implemented for use in three-dimensional flows. High-speed analog processing produces the turbulence data in real time, including all double correlations. A 2-mm diameter miniature probe has been developed. The system has been tested in reference flows and used in a curved boundary layer.

DD FORM 1 JAN 73 1473

UNCLASSIFIED 400 774

Abstract

Documentation of the structure of turbulence in three-dimensional flow fields requires extensive data-taking which is time-consuming and expensive. A triple-wire hot-wire anemometer system was developed at Stanford which produced electrical signals proportional to the instantaneous values of the u, v, and w components of velocity in laboratory coordinates. Digital processing was required, however, to extract the turbulence information.

The present project was to construct an analog processor which would be compatible with the existing triple-wire system and to test the system both electrically and in a reference flow field.

It is demonstrated, by the data herein, that the mean velocity can be measured within 1.4% so long as the incident vector lies within 30° of the axis of the probe. Turbulent shear stress can be measured within 2.5% so long as the incident velocity vector is within 20° of the axis. No reference flows are available for $\overline{u'^2}$, $\overline{v'^2}$, and $\overline{w'^2}$, but the values returned by the Triple-Wire Processor are reasonable and in agreement with prior results.

Wiring diagrams and electrical performance test results are included.

A demonstration data set is presented, taken in a convexly curved boundary layer.

Acknowledgments

The authors acknowledge the support of the Air Force Office of Scientific Research for their grant, Number AFOSR 78-3597, which supported the work reported herein for a seven month period from May 1, 1978, until December 1, 1978. The contract was administered by Dr. Samaris on behalf of AFOSR.

Table of Contents

Figure List

Chapter I

TRIPLE-WIRE THEORY AND BACKGROUND

Current research programs in turbulent boundary layer heat transfer involve situations in which the turbulence levels are very high (perhaps 25-50%) with the direction of the mean flow either unstable or uncertain (within ±15°). Examples would be flows over surfaces cooled by injection through discrete holes (turbine blade cooling), or flows past large roughness elements, or flows over backward-facing steps. In each of these cases, large amounts of data are needed in order to map the turbulence fields, and, since no proven predictive model yet exists, it is not yet known which one or two properties are most relevant. One would like to document as much of the structure as possible, to assure capturing the most important properties.

The flows of interest here are laboratory flows, of relatively large scale, operating at essentially ambient conditions of temperature and pressure and at velocities between 5 and 50 m/s. The usual approach is to measure the time-averaged output and the mean square of the fluctuating output from a hot wire at each of several consecutive positions (or from two or more wires at the same time) and then deduce the turbulence components by solving a set of simultaneous equations involving these time-averaged outputs.

The ambiguities which arise when the flow direction is unknown or the turbulence is large are brought on by the fact that the signal from a hot wire is sensitive to all three components of the velocity relative to the wire.

To illustrate the nature of the problem, it is instructive to examine the equations necessary for the usual treatment of a flow of unknown direction. The relation between the effective velocity and the velocity components will be taken as in Eqn. (1), from Jorgensen (1971), with the nomenclature as shown in Fig. 1, using x', y', z', a right-handed set defined with respect to the axis of the wire and the plane of the prongs. If the two prongs are of different length, then the longer prong is assumed to be at the higher positive y' value.

$$U_{eff}^2 = X^2 + k_2^2 Y^2 + k_2^2 Z^2 \qquad (1)$$

In the above equation X, Y, Z are the velocity components in the directions of the wire coordinates x', y', and z', respectively, and k_1 and k_2 are directional sensitivities of the wire. Fig. 2 shows a single rotatable slant-wire probe whose longitudial axis is fixed with respect to the laboratory coordinates x, y, and z. The angle ϕ is the slant angle, measured in the plane of the prongs, between the wire and a line perpendicular to the prongs. The roll angle is taken to be positive in the clockwise direction looking upstream: *Fig. 2 shows a negative roll position.*

Any instantaneous velocity R can be considered to be the resultant of three components measured in the lab coordinate system. The x, y, z components will be named U, V, and W, respectively. These components can each be resolved into components X, Y, Z with respect to the coordinate system of the wire, if α and ϕ are known. The result can be used to express the effective velocity on the wire in terms of the components of velocity measured in lab coordinates. This result is given as Eqn. (2).

$$U_{eff}^2 = A(U^2) + B(V^2) + C(W^2) + D(UV) + E(VW) + F(UW) \qquad (2)$$

where

$$A = \cos^2\phi + k_1^2 \sin^2\phi$$
$$B = (\sin^2\phi + k_1^2\cos^2\phi)\cos^2\alpha + k_2^2\sin^2\alpha$$
$$C = (\sin^2\phi + k_1^2\cos^2\phi)\sin^2\alpha + k_2^2\cos^2\alpha$$
$$D = (1 - k_1^2)\sin 2\phi \cos\alpha$$
$$E = -(\sin^2\phi + k_1^2\cos^2\phi - k_2^2)\sin\alpha \quad \text{and}$$
$$F = -(1 - k_1^2)\sin 2\phi \sin\alpha$$

In Eqn. (2), each velocity can be written as the sum of a mean and a fluctuating part:

$$U = \overline{U} + u'$$

$$V = \overline{V} + v'$$

$$W = \overline{W} + w'$$

and

$$U_{eff} = \overline{U}_{eff} + u'_{eff}$$

If these definitions are substituted in Eqn. (2), a very complicated equation results. In the classical time-averaged method, the only quantities recorded are $\overline{U}_{eff}$ and $\overline{u'^2_{eff}}$ and all turbulence information must be deduced from those values.

Equation (2) can be brought to a theoretically solvable form by a Taylor's series expansion of both sides using the assumptions that the flow has both a strongly preferred direction and also low fluctuations (i.e., $\overline{V}$, $\overline{W}$, and u', v', and w' are each at least one order of magnitude smaller than $\overline{U}$). The simplified equations are given below:

$$\begin{aligned}\overline{U}_{eff} = \frac{1}{2\sqrt{A}\,\overline{U}}\Big[&(2A\overline{U}^2 + B\overline{V}^2 + C\overline{W}^2) + (D\overline{UV} + E\overline{VW} + F\overline{UW}) \\ &+ (A\overline{u'^2} + B\overline{v'2} + C\overline{w'^2}) \\ &+ (D\overline{u'v'} + E\overline{v'w'} + F\overline{u'w'})\Big] \; .\end{aligned} \tag{3}$$

$$\begin{aligned}\overline{u'^2_{eff}} = \frac{1}{4A}\Bigg[&\left(4A^2 + D^2\frac{\overline{V}^2}{\overline{U}^2} + F^2\frac{\overline{W}^2}{\overline{U}^2} + 4AD\frac{\overline{V}}{\overline{U}} + 4AF\frac{\overline{W}}{\overline{U}} + 2DF\frac{\overline{VW}}{\overline{U}^2}\right)\overline{u'^2} \\ &+ \left(D^2 + 4B^2\frac{\overline{V}^2}{\overline{U}^2} + E^2\frac{\overline{W}^2}{\overline{U}^2} + 4BD\frac{\overline{W}}{\overline{U}} + 2DE\frac{\overline{W}}{\overline{U}} + 4BE\frac{\overline{VW}}{\overline{U}^2}\right)\overline{v'^2} \\ &+ \left(F^2 + E^2\frac{\overline{V}^2}{\overline{U}^2} + 4C^2\frac{\overline{W}^2}{\overline{U}^2} + 2EF\frac{\overline{V}}{\overline{U}} + 4CF\frac{\overline{W}}{\overline{U}} + 4CE\frac{\overline{VW}}{\overline{U}^2}\right)\overline{w'^2} \\ &+ \left(4AD + 4BD\frac{\overline{V}^2}{\overline{U}^2} + 2EF\frac{\overline{W}^2}{\overline{U}^2} + (8AB+2D^2)\frac{\overline{V}}{\overline{U}} + (4AE+2DF)\frac{\overline{W}}{\overline{U}}\right. \\ &\left. + (2DE+4BF)\frac{\overline{VW}}{\overline{U}^2}\right)\overline{u'v'} + \Bigg(4AF+2DE\frac{\overline{V}^2}{\overline{U}^2} + 4CF\frac{\overline{W}^2}{\overline{U}^2}\end{aligned} \tag{4}$$

(cont.)

$$+ (4AE+2DF)\,\frac{\overline{V}}{\overline{U}} + (8AC+2F^2)\,\frac{\overline{W}}{\overline{U}} + (2EF+4CD)\,\frac{\overline{V}\overline{W}}{\overline{U}^2}\Bigg)\,\overline{u'w'}$$

$$+ \Bigg(2DF+4BE\,\frac{\overline{V}^2}{\overline{U}^2} + 4CE\,\frac{\overline{W}^2}{\overline{U}^2} + (2DE+4BF)\,\frac{\overline{V}}{\overline{U}}$$

$$+ (4CD+2EF)\,\frac{\overline{W}}{\overline{U}} + (8BC+2E^2\,\frac{\overline{V}\overline{W}}{\overline{U}^2}\Bigg)\,\overline{v'w'}\Bigg] + O(3) \quad .$$

Even with these assumptions, the resulting equations are quite complicated. Aligning the probe with the flow direction sets $\overline{V}$ and $\overline{W}$ to zero and, in cases where there is symmetry, ($\overline{u'w'} = 0$ and $\overline{v'w'} = 0$), the equations reduce to the following form, which is generally used for rotatable slant wires:

$$\overline{U}_{eff} = \sqrt{A}\,\overline{U} + O(2) \tag{5}$$

$$\overline{u'^2_{eff}} = A\,\overline{u'^2} + \frac{D^2}{4A}\,\overline{v'^2} + \frac{F^2}{4A}\,\overline{w'^2} + D\,\overline{u'v'} + O(3) \quad . \tag{6}$$

One measures $\overline{U}_{eff}$ and $\overline{u'^2_{eff}}$ in each of four different positions, thus obtaining enough equations to solve for these unknowns.

The most important problem in 3-D flows is that the direction of the mean flow is unknown. This direction can be found with one of the following ways. Johnston (1970) measured the local pitch and yaw angles for the mean velocity with a Conrad probe. Reynolds stresses were then obtained from a horizontal wire and a rotatable cross-wire aligned according to the known flow direction. The low-fluctuation assumption was then invoked and the turbulence quantities measured. Moussa and Eskinazi (1975) tried to measure the mean flow direction by using a rotatable slant wire. Making use of the directional properties of hot wires, they calibrated the probe for all possible angles and prepared detailed charts which included the flow angles as functions of four mean voltages obtained at different rotations of the probe. Delleur (1966) used a cross-wire to measure the flow direction. He argued that the cross-wire technique is twice as accurate as the single-wire technique. Both methods require the use of a hot-wire calibration curve for flow-direction measurement and frequent calibration of the hot wire to renew the calibration charts.

Some other 3-D hot-wire methods were developed which do not require the flow direction to be known a priori. Majola (1974) gives a hot-wire method (rotatable slant wire or cross-wire) for measuring the three mean components of the velocity and six Reynolds stresses without knowing the flow direction. His equations are valid when there is a strongly preferred mean flow direction and for low fluctuations. Hoffmeister (1972) describes a scheme which employs a single rotatable slant wire to obtain three mean velocities and six Reynolds stresses. In this scheme the interpretation of the anemometer voltages is based on calibrations of the probe in the entire range of angles between the wire and the flow existing during measurements.

None of the preceding methods seemed practical for taking large amounts of data. Further, the accuracy with which the higher-ordered terms can be measured is seriously limited. As the number of terms retained from Eqn. (4) increases, the number of independent realizations required increases; thus the number of probe rotational positions increases, and the independence of the realizations diminishes.

The problem lies, basically, in the time-averaged approach to turbulence measurement. With one or two wires, one does not have enough information to solve for the instantaneous velocities, and hence time-averaging is required.

The Present Approach

Three orthogonal hot wires provide enough information to solve for the instantaneous velocity without time averaging, and some commercial circuitry is available for this purpose. Such a scheme was used by Zimmerman and Abbott (1975) to measure the Reynolds stresses in a 3-D boundary layer created by a flat plate skewed with respect to the oncoming flow. A triaxial probe was used with a commercial analog processor, yielding the mean components and Reynolds stresses.

The present approach differs mainly in the frequency response capabilities of the circuitry and the fact that the directional properties of the individual wires can be used, instead of a global assumption. The present system provides more output information, but that is of secondary importance.

The first requirement is a triple-wire probe whose wires form an orthogonal set. For such a probe, the X component for one wire is the Y component for another and the Z component for the third. Such a probe is commercially available either from the DISA Corporation or from Thermosystems, Inc.

The DISA triaxial wire probe, shown in Fig. 3, has three wires with separate ground leads, to be driven by three separate anemometers. The wires are mutually orthogonal and can be used to define a left-handed coordinate system, as shown. It is necessary to describe the coordinate system as left-handed, with one axis parallel to each of the wires, and to name the axes and number the wires as shown in Fig. 3, in order that the equations which follow will produce the proper sign for each velocity component. This results principally from the fact that the u-component of velocity is directed back along the stem of the probe when positive. The probe axis lies inside the quadrant bounded by +x', +y', and +z'.

The sensors provided by DISA are 3.4 mm long, with 5 micron Pt-plated tungsten wires, plated at the ends with copper and gold to leave a sensitive length of 1.25 mm. In the early phases of the present work, bare Pt-plated tungsten wires were used without gold plating, giving 3.2 mm active length. The three wires form a cone of half-apex angle 54.7° around the axis of the probe stem. With the special prong structure of the probe, the effective velocity indicated by each wire is related to the velocity components in this coordinate system in the following manner.

$$\begin{aligned} U_{eff_1}^2 &= k_{11}^2 X^2 + Y^2 + k_{21}^2 Z^2 \\ U_{eff_2}^2 &= k_{22}^2 X^2 + k_{12}^2 Y^2 + Z^2 \\ U_{eff_3}^2 &= X^2 + k_{23}^2 Y^2 + k_{13}^2 Z^2 \end{aligned} \tag{7}$$

The linearized effective voltages (linearizer outputs) are related to the effective velocities as follows:

$$U_{eff_1} = A_1 + B_1 E_{eff_1} \tag{8}$$

(cont.)

$$U_{eff_2} = A_2 + B_2 E_{eff_2} \tag{8}$$

(cont.)

$$U_{eff_3} = A_3 + B_3 E_{eff_3}$$

In Eqns. (8), the A's and B's are constants, obtained from calibrations of the wires.

Equations (7) have three unknowns -- the instantaneous velocities in the wire coordinates -- which can be obtained from the equations shown below:

$$\begin{bmatrix} X^2 \\ Y^2 \\ Z^2 \end{bmatrix} = \begin{bmatrix} k_{11}^2 & 1 & k_{21}^2 \\ k_{22}^2 & k_{12}^2 & 1 \\ 1 & k_{23}^2 & k_{13}^2 \end{bmatrix}^{-1} \begin{bmatrix} U_{eff_1}^2 \\ U_{eff_2}^2 \\ U_{eff_3}^2 \end{bmatrix} \tag{9}$$

$$\begin{bmatrix} X^2 \\ Y^2 \\ Z^2 \end{bmatrix} = \begin{bmatrix} k_{11}^2 & 1 & k_{21}^2 \\ k_{22}^2 & k_{12}^2 & 1 \\ 1 & k_{23}^2 & k_{13}^2 \end{bmatrix}^{-1} \begin{bmatrix} A_1 + B_1 E_{eff_1}{}^2 \\ A_2 + B_2 E_{eff_2}{}^2 \\ A_3 + B_3 E_{eff_3}{}^2 \end{bmatrix} . \tag{10}$$

Once the instantaneous velocities in the wire coordinates are obtained, the instantaneous velocities in the laboratory coordinates can be obtained easily with a transformation of coordinates.

$$\begin{bmatrix} U \\ V \\ W \end{bmatrix} = N \begin{bmatrix} X \\ V \\ Z \end{bmatrix} \tag{11}$$

where N is the coordinate transformation matrix from wire coordinates to laboratory coordinates. The solution to Eqns. (11) is a set of three instantaneous velocities in the laboratory coordinate system.

The Three-Dimensional Turbulent Flow Analyzer

The intent was to develop a low-cost, stand-alone unit with which one could process the signals from three linearized anemometers. The objective was to obtain information concerning both the amplitude and relative phase of the three components of the instantaneous velocity, over the frequency range from D.C. up to 10 kHz. The "low-cost, stand-alone" requirement was important, since it was intended to make these units available to each of several experiments which might all be running at the same time.

The system finally adopted uses analog processing, although digital techniques were considered. The principal argument which led to selection of the analog scheme was that acceptable accuracy (2% to 3%) could be obtained over an acceptable frequency range (4 Hz to 10 kHz) at much lower cost than by using digital processing. The trend in digital systems has since been towards higher speed and lower cost, and it may soon be economically feasible to do these calculations digitally.

An analog device was built to solve Eqns. (10) and (11) using high-speed analog components. All quantities were magnitude-scaled using $(U_{eff})_{max}$, the value which resulted in the maximum output of the linearizer. The coefficients A and B in Eqn. (10) are the same for each wire, since A and B are functions of the minimum and maximum velocities of the calibration range for the triple-wire probe. Different values of k_1 and k_2 can be set for each wire.

Figure 4 shows the control panel of the Flow Analyzer (lower panel) and the Coordinate Rotation Unit (upper panel). On the Flow Analyzer panel, three potentiometers are used for setting the B coefficients even though the three values are the same, because of circuitry requirements. The nine potentiometers for the coefficients of the inverse Jorgensen matrix are shown, each with a pair of test points for checking its value. The meter provides a continuous display of R/C, the time-averaged value of the magnitude of the velocity vector. The outputs of the Flow Analyzer are the three normalized velocity components in wire coordinates X, Y, Z plus the value of R/C, the root sum square of the components. The Coordinate Rotation Unit accepts the X, Y, Z inputs and calculates the values of $U, V,$ and W, the normalized velocity components in laboratory coordinates, using nine potentiometers whose values are set according to the wire position.

The flow diagram of the Flow Analyzer and Coordinate Rotation unit are shown in Fig. 5.

Electrical performance tests were conducted on each unit, to ensure that no phase shift or attenuation occurred. The Flow Analyzer and Coordinate Rotation Unit show a phase shift less than 2° up to 20 kHz, with signal attenuation of about 0.1% (maximum).

Fluid Mechanic Qualification Tests

The Thermosciences Laboratory in the Mechanical Engineering Department of Stanford University has a two-dimensional channel which gives fully developed mean velocity and turbulence profiles up to at least the second-order turbulence quantities. The performance characteristics of this channel have been fully explored; it has been used by almost all recent experimenters to calibrate their hot-wire technique, their probes, and their system. The Flow Analyzer and Coordinate Rotation Unit were tested in this channel to qualify their performance and to explore their limitations for turbulence measurements.

For the qualification tests, a rotatable probe was mounted in a two-axis probe traverser so that it could be rotated around its axis (roll angle α) and also tilted (pitch angle ω) against the approaching flow, as well as traversed to several different distances from the wall. By measuring at several distances from the wall, the system performance was recorded both for high shear regions (near the wall) and zero shear regions (at the centerline of the channel). The outputs were compared with the outputs of the other acceptable methods of measurement in the channel (single horizontal wire, pitot tube measurements, and linear shear stress distribution calculated from the pressure gradient along the channel).

The two-dimensional channel is 6.35 cm wide and 117 cm high. The experiments were made with air flow at ambient conditions and with a centerline speed of 11.2 m/sec.

In Fig. 6 the values of $\overline{U}$ (the streamwise mean velocity) obtained from a pitot probe and from the triaxial probe are compared. The pitot probe was modified to create the same kind of stem blockage effect in the channel as did the triaxial probe. In this test the probe was set to zero roll ($\alpha = 0^0$) and the axis was aligned with the flow ($\omega = 0^0$). The readings of the pitot probe were corrected for shear displacement effect and for turbulence level. The maximum difference between the two probes occurs near the wall -- about

2.4%. The difference diminishes rapidly as the distance from the wall increases. The difference near the wall may be due to the finite size of the triaxial probe interacting with the velocity gradient.

Next, the effect of rotation of the probe around its axis was investigated. When the probe axis is aligned with the flow direction ($\omega = 0^0$), rotation around its streamwise axis should not affect the result if the velocity is uniform, but may affect the result in a shear flow. To investigate this, the probe was aligned with the flow direction ($\omega = 0^0$), and for each transverse position across the tunnel the probe was rotated around its axis to the values of $\alpha = 0°$, 90°, 180°, and 270°. This angle range covers the extreme positions for the wires and exposes different configurations of wires to the shear at different angles.

Figure 7 shows the three mean velocity components ($\overline{U}$, $\overline{V}$, and $\overline{W}$) as a function of the distance from the wall for several values of the roll position, α. Roll around the probe axis does not affect the $\overline{U}$ values. The effect on $\overline{V}$ abd $\overline{W}$ is small, but not negligible. In this figure, $\overline{V}$ and $\overline{W}$ values are also plotted to the same scale as $\overline{U}$. The values of $\overline{V}$ and $\overline{W}$ should be zero but some deviation from zero is observed within the shear region. The most meaningful comparison for error in $\overline{V}$ and $\overline{W}$ is to compare them to the $\overline{U}$ at the same location. The largest deviations occur at points near the wall. For $\alpha = 0$, $\overline{V}/\overline{U} = 1\%$; and for $\alpha = 270^0$, $\overline{W}/\overline{U} = 4.5\%$. These deviations from zero become smaller as the distance from the wall increases. In the zero gradient region at the centerline there is no deviation.

Figure 8 shows the turbulence kinetic energy and shear stress distributions as a function of the distance from the wall for several values of the roll angle. The shear stress ($-\overline{u'v'}$) measurements are compared with the shear strss distribution calculated from the pressure gradient along the channel (dp/dx). As is seen, all the experimental data lie inside the ±20% error band, but at angles $\alpha = 90^0$ and $\alpha = 270^0$ the deviations are much smaller; therefore, one would like to measure $-\overline{u'v'}$ at these angles. The measured turbulent kinetic energy is not much affected by the roll. The largest difference between results occurs at the high shear region near the wall; it is about 3.5%. In the zero shear region there is no effect of roll.

Figure 9 shows the diagonal Reynolds stress components ($\overline{u'^2}$, $\overline{v'^2}$, $\overline{w'^2}$) as a function of the distance from the wall, normalized with centerline velocity. The streamwise normal stress $(\overline{u'^2})$ does not seem to be affected much by roll around the probe axis, even in the high shear regions near the wall. On the same figure, the $\overline{u'^2}$ distribution obtained with a conventional single horizontal wire is also given, and its agreement with the triaxial wire data is not bad. The other normal Reynolds stresses $(\overline{v'^2}$ and $\overline{w'^2})$ are affected by the roll angle, especially in the high shear region, but the data collapse on each other quickly as the shear decreases. In the zero shear region on the centerline there are no deviations. One important observation is that, at a certain α value, if $\overline{v'^2}$ reads high compared to the value at $\alpha = 0^0$, then $\overline{w'^2}$ reads low, or vice versa, while $\overline{u'^2}$ does not change much with α. This combination leads to q^2 values which are quite insensitive to the changes in α, a fortuitous result for the measurement of q^2 -- the main interest of the general research.

The data discussed above are enough to qualify this system for measurements when the probe axis is aligned with the flow direction, but one of the most important objectives of this research was to find a method which would work in a flow of unknown direction. To investigate this, the probe axis was tilted against the approaching flow direction (ω), again in the 2-D channel, and the calibration repeated. Some rotations around the probe axis (α) were also tested to see the combined effect of both α and ω. The results are discussed in the following paragraphs.

Figure 10 shows the three mean velocity components as a function of distance from the wall for several values of the angle between the flow and the probe axis (ω). Here the value of α was held constant, because it was seen above that the mean velocities were not much affected by the roll angle. For $\overline{U}$ up to $\omega = 20^0$ the data collapse on top of each other and the deviation for $\omega = 30^0$ is not very large. The largest deviation at this angle is about 3.5% in the high shear region near the wall, and about 2% in the zero shear region. Deviation is calculated as the difference between two extremes, not from the pitot probe data. This result means that mean velocity can be measured with good accuracy if the approaching flow direction is within ±30° of the probe axis; i.e., one does not have to know the flow direction better than within a cone of half apex angle 30° around the probe axis to measure the mean velocity with acceptable accuracy. (If $\overline{V} = 0.1\,\overline{U}$, this will give an angle of about ±6°.) As the angle between the flow direction and the probe axis increases, the errors in $\overline{V}$ and $\overline{W}$ also increase (ideally, their values should be zero).

In Figure 11 the turbulence kinetic energy (TKE) and shear stress are plotted for several values of roll angle (α) and pitch angle (ω). In the TKE plot the line at the center is faired through the data at $\omega = o^0$, $\alpha = 0^0$ (this measurement should be the one closest to reality). The other lines denote the ±10% and ±15% error bands around the reference. Again, the data points converge rapidly as the distance from the wall increases. Deviations are much smaller in the zero shear region. In the same figure, the q^2 distribution for $\alpha = 90^0$, $\omega = 20^0$ is shown, to demonstrate the increase in deviation as ω increases. Another important point to observe from this figure is that for $\alpha = 90^0$ and $\omega = 10^0$ the data lie very close to the center profile. This shows that, depending on the quantity being measured, there are angle combinations α and ω for which the measurement cone can be enlarged. For example, for $\alpha = 90^0$ and $\omega = 10^0$ and 20°, it appears that even in the highest shear region q^2 can be measured within 10% or 12% inside a cone of 10° half apex angle around the probe axis. The deviations in q^2 are not like uncertainty scatters, but rather have a preferred direction. It may be possible to devise a scheme to correct the data based on the first estimate of the flow direction, to improve the accuracy. In the shear stress part of Fig. 11, the straight line in the middle of the figure is the shear stress distribution obtained from the pressure gradient in the streamwise direction. The other straight lines are the boundaries for ±10% and ±15% error. Most of the data up to the angle $\omega = 10^0$ lie within 10% error band, except a few points near the wall for angles $\alpha = 270^0$ and $\alpha = 90^0$. Almost all the data, including $\omega = 15\%$ and $\alpha = 0^0$, lie within the ±15% error band. The shear stress $-\overline{u'v'}$ can be measured within 10% within a cone of half apex angle 10° and within 15% inside a cone of half apex angle 15%, except very near the wall.

Conclusions Regarding the Triple-Wire Processor and Coordinate Rotation Unit

It has been shown that an analog processor can be used to deduce the three instantaneous components of velocity in real time $(\overline{U}, \overline{V},$ and $\overline{W})$ using three linearized hot-wire anemometers. The electronics have been shown capable of operation with less than 2° phase shift and less than 0.1% attenuation over the frequency range from D.C. to 20,000 Hz.

From the data-reduction stantpoint it remained to develop a post-processor unit which would operate on the three independent inputs to produce the required turbulence data. The first application of the Flow Analyzer was made with an analog-to-digital interface operating on U, V, and W, and with fully digital calculation of all shear stress and turbulence data. The prospect of an analog device for such operations was attractive, and this desire formed the basis of the proposal whose results follow.

The fluid mechanic calibrations established the band of error associated with measurement of the turbulence quantities. Some of these errors may be related to the fluid mechanics around the probe tip (flow distortion caused by the probe), some are electrical (imperfections in gain and nonlinearities in the system), and some reflect imperfect description of the directional sensitivity of the probe by the Jorgensen coefficient matrix.

The work done under the present contract was aimed at: (1) developing an all-analog post processor, (2) reducing the errors in measurement, (3) and miniaturizing the triple-wire probe.

The prior work on the triple-wire processor was reported by Yavuzkurt (1977). The equations and data of this chapter are from his work.

Chapter II

THE POST-PROCESSOR

The triple-wire processor (Flow Analyzer and Coordinate Rotation Unit) produces three signals, one proportional to each of U, V, and W, the instantaneous velocities in laboratory coordinates x, y , and z.

The function of the Post-Processor Unit is to separate the instantaneous segments into mean and fluctuating components and then to form certain products of the fluctuations. The separation between mean and fluctuating quantities requires a decision as to the cut-off frequency of the low-pass filter (i.e., the frequency above which changes will be regarded as part of the turbulence). Various filter designs are available, with different frequency response characteristics, and the filter design must be chosen for best overall system performance, not simply a sharp cut-off at the chosen frequency. In particular, it is important that the filter not alter the phase relationships between components having different frequencies.

In the following sections, the basic flow diagram will be presented, along with the rationale for selecting the filters and multipliers. The system wiring diagram and expected electrical performance will be noted. Finally, the electrical qualification tests will be documented.

Filter Units

Separation of an input signal into "mean" and "fluctuating" components is achieved by bringing the signal to two filter units, in parallel, one low-pass and one high-pass unit. The filter unit design requires selection of a cut-off frequency, based upon the probable nature of the input signal.

Figure 12 shows three spectral scans of the turbulence in a rough-wall boundary layer, typical of the signals which may be encountered. Three different wire lengths were used (ℓ/d = 90, 250, and 600) to document the effect of length-averaging on the apparent spectrum. The function $f_u(n)$ is down to about 0.1 at 7 kHz, from a high value of 110 at 20 Hz. Thus, to capture the principal components requires a high-frequency capability of about 8 kHz without error.

The low-frequency end of the spectrum was not investigated in the spectral scans, due partly to equipment limitations and partly to the fact that energy considerations were not felt to be the most important aspects at the low-frequency end. The decision was made to push the cut-off frequency to as low a value as possible, to retain the ability to observe the phase relationship between u, v, and w, as large-scale structures moved past the probe. A single-pole filter introduces phase shifts between the input and output signals both at the high- and low-frequency end. As the cut-off frequency is pushed lower and lower, the phase shift at the high-frequency end of the range also moves down in frequency. The cut-off frequency was selected to be 0.159 Hz ($\frac{1}{2}\pi$ Hz) in order to limit the phase shift at 8 kHz to 1 degree. The phase shift window of the single-pole filter unit is shown in Fig. 13. Approximatly 1° phase shift will be introduced at 10 Hz and at 8 kHz.

The attenuation characteristics of the high-pass filter units were determined for various combinations of AC and DC voltages and frequencies (sine wave AC), to search for cross-talk between AC and DC inputs. Circuit characteristics require that the input signal remain less than 10 volts for all operating conditions. During all tests of the filters and the multipliers, as the DC component of the input was raised, the AC component was reduced to keep the instantaneous peak voltage between 0 and 10 volts. The attenuation of the AC components will be discussed in terms of the AC- coupled RMS voltage levels (i.e., no sensitivity to the DC component). Fig. 14 shows the AC data. Attenuation was less than 1% everywhere within the operable domain. There was no discernible effect of DC level on the AC attenuation.

The attenuation characteristics of the low-pass filter units were also determined for various combinations of AC and DC voltages and frequencies. Again, the purpose was partly to search for cross-talk between the AC and DC inputs. The attenuation of the DC component will be discussed in terms of the Absolute Value of the output and input, since the filters change the sign. Fig. 15 shows the DC attenuation, again within 1% from 1Hz to 10 kHz and showing no discernible interaction between the AC and DC signals. Two sets of filters were tested, with the same outcome: less than 1% attenuation anywhere within the operable domain.

The schematic wiring diagram of the high- and low-pass filter units is shown in Fig. 16.

Multiplier Units

Multiplication of the fluctuating components from the input channels will be used to measure the turbulent shear strsses. The multipliers must function independently of frequency up to 10 kHz, both with respect to phase shift and attenuation. The multiplier design shown in Fig. 16 was tested by providing two known signals to its input and measuring the output. The input signals were mixed AC and DC, with a 10 volt peak. Output voltages were measured with an integrating digital voltmeter (for the DC component), an AC-coupled RMS meter (for the AC component), and a phase meter. The test arrangement is shown in Fig. 17. Figs. 18 and 19 present the AC and DC attenuation characteristics of the multiplier. About 7% scatter was observed in the low-voltage results, but this was attributed mainly to uncertainties introduced by the RMS voltmeter used in measuring the input signals.

Intermediate Amplifier

Tests of the prototype post-processor showed too low a signal-to-noise ratio in the turbulence branch when processing signals whose turbulence component was less than 10% of the mean.

The difficulty was caused by the fact that the multipliers used in this circuit form the product of A and B as - AB/10, to guard against overvoltage on high inputs. As a consequence, when used with low inputs, the multiplier output is too low.

A 10X fixed-gain amplifier was inserted into each branch, with a disable switch, just after the high-pass filter. This offered the operator the option of increasing the signal strength, when needed. The schematic is shown in Fig. 20.

Differentiator, Gain Block, and Summing Amplifier

A time differentiator circuit is required in the evaluation of dissipation, $D/Dt(u^2)$. Although this portion of the circuit has not yet been implemented, the design work has been completed. The differentiator circuit is shown in Fig. 21, along with a fixed-gain block for improving the signal-to-noise ratio.

Summing amplifiers are used in several locations in the Post Processor. Their schematic is shown in Fig. 22.

Post-Processor Flow Diagram

At the conclusion of the electrical tests, the Post-Processor Unit was incorporated into the Triple-Wire Processor. Fig. 20 shows the assembled Triple-Wire Processor. The center panel is the Flow Analyzer board, which accepts inputs from three linearized anemometers and produces three signals, one proportional to each component of the instantaneous velocity referred to the coordinate system of the three wires. The output of the Flow Analyzer is passed to the Coordinate Rotation Unit, at the top, which produces signals proportional to the components of velocity in laboratory coordinates. These signals are led to the Post-Processor Unit, at the bottom, and the individual signals extracted either from the test points at the front panel or from a computer-compatible connector strip on the back of the chassis.

The system occupies three panels in a 19-inch rack in its present form, but could likely be reduced to two panels or even to one panel if the "rarely used" adjustments were placed on the back panel instead of the front.

The flow diagram of the Post-Processor is shown in Fig. 24 and its schematic in Fig. 25. The three inputs (U, V, and W) are divided into mean values ($\overline{U}$, $\overline{V}$, and $\overline{W}$) and fluctuating values (u', v', and w') by high- and low-pass filter units. Both the mean and fluctuating values are available for external reading, both through the front panel and through a computer connection.

The fluctuating signals may or may not be multiplied by 10 at the discretion of the operator. This feature improves the signal-to-noise ratio of the turbulence data for low-level inputs.

The amplified fluctuating output from each channel is sent to three different multipliers in parallel, so that, from an input of u, v, and w, each of the possible products is formed: u'u', u'v', and u'w'.

The instantaneous products are available for external reading either through the front panel or through a computer connection.

The instantaneous products are each sent through low-pass filters, producing output proportional to their time-averaged values. These are available for external reading either through the front panel or through a computer connection.

The instantaneous values of the squares of the fluctuations $(u'^2, v'^2,$ and $w'^2)$ are collected through summing amplifiers to yield the instantaneous value of q^2, which is then sent through a low-pass filter to produce $\overline{q^2}$. Both the instantaneous and the time-averaged values of q^2 are available either at the front panel or at the computer tie.

The board design includes a fourth channel, for temperature measurement, and has provision for implementing triple correlations, including temperature fluctuations. Neither of these features had been implemented as of the time of this report.

The Post-Processor board was tested electrically by providing known voltages to the u, v, and w input terminals and measuring the outputs u', v', w', u'^2, v'^2, w'^2, and $\overline{u'^2}$, $\overline{v'^2}$, $\overline{w'^2}$, as well as $u'v'$ and $\overline{u'v'}$. No error as large as 3% was found, and all but one reading was within 2%. The test signal was 2.00 volts DC plus 0.688 volts RMS AC at a frequency of 4938 Hz. The X10 multiplier amplifier was used to boost the fluctuating signals, and should be used when it does not cause saturation in the multipliers. A tentative criterion is that the X10 multiplier should be used whenever $\overline{u'v'}/10$ would be less than 0.3 volts without the multiplier.

Chapter III

OPERATION OF THE TRIPLE-WIRE PROCESSOR

This section describes the operating and calibrating procedures followed in using the triple-wire processor. It is assumed that the reader is familiar with the use of conventional hot-wire anemometers and linearizers.

The following general steps will be followed:

- Calibrate the anemometers and linearizers.
- Set up the control potentiometers of the Flow Analyzer.
- Set up the control potentiometers of the coordinate Rotation Unit: one must decide whether or not to turn on the 10X amplifier in the turbulence branch.
- Interpret the output.

Calibration of the Anemometers and Linearizers

The probe was placed in the calibration tunnel with its axis parallel to the flow. The effective velocity, U_{eff}, applied to each wire was calculated from the probe geometry, using the Jorgensen coefficient matrix. Each wire is at the same angle, 54.79°, with respect to the approach velocity; hence using the Jorgensen form with $k_1 = 0.15$ and $k_2 = 1.02$ yields:

Calibration Condition:

$$U_{eff}^2 = U_{app}^2 \cos^2 54.74 \{1 + k_1^2 + k_2^2\} \tag{12}$$

or:

$$U_{eff} = 0.829\, U_{app} \tag{13}$$

Approach velocity (synonymous with stream velocity) was calculated using Bernoulli's equation based on measurements of total and static pressure. A Combist micromanometer was used for measuring the dynamic head.

The three wires of the probe are nearly identical, except for manufacturing tolerances and probe misalignment tolerances; hence it is not surprising that the three calibrations of E versus U_{eff} are very similar --

typically only 0.2 to 0.3% difference in bridge output. Subsequent processing and calibration steps are much easier if the three bridge outputs are matched instead of allowed to remain different by such small amounts. Matching of the bridge outputs is accomplished by small changes in the hot resistance (overheat ratio) of two of the bridges. Typically, one would keep the "middle calibration" and adjust the other two, to minimize the difference in overheat ratios from wire to wire.

The linearizer used in the present embodiment is the TSI 1052 (or 1072), which allows pre-calculation of four coefficient values, based upon the U_{eff} versus E output calibration. With a "universal" calibration for the three wires, the same coefficients are used on all of the linearizers. Zero and span settings on the linearizers are adjusted for 0.000 and 10.000 volts according to standard practice, using a common value of voltage to each linearizer for the zero setting, and another common input voltage again for the span adjustment.

Experience has shown that lower uncertainties are introduced by trying to individualize the three channels than by this technique of compensating by small changes in the overheat ratio.

During the course of testing, the temperature of the stream may change and introduce errors into the hot-wire system. Linearized systems are particularly sensitive, since they produce a 0-10 volt signal for only a small change in bridge output voltage (typically only 0.3 volts), although the level of voltage is high (typically 3 volts). A 1% change in level (3.0 volts) causes a change equivalent to a 10% change in velocity, as a consequence of the amplification induced by the linearizer. It is necessary, therefore, to do one of two things: either (1) stabilize the temperature of the stream, or (2) devise a compensating technique.

The technique used in the prsent work is one of compensation by adjustment of the overheat ratio so as to keep the relationship between U_{eff} and E invariant. If that relationship is fixed, then so is the relationship between the linearizer output and the effective velocity -- and this is the final outcome. It is assuredly easy to preserve the E vs. U_{eff} relationship at a single value of U_{eff}. Experimental evidence was needed, however, that an adjustment made at high velocity would preserve the shape of the E versus E_{eff} calibration at lower velocities as well. Calibrations were made at two temperatures about 3° apart, adjusting the hot resistance to yield the same value of E at $U_{eff,max}$. The two calibrations were indistinguishable from one another. The techniques described above allow the three bridges and linearizers to be set up at the beginning of a run, and readjusted periodically during a long test by the simple expedient of returning the probe to a reference location and adjusting the hot resistance until the original output is regained.

Setting the Control Potentiometers on the Flow Analyzer

The Flow Analyzer accepts, as its inputs, three BNC cables, one bearing the signals from each of the three wires.

The first controls which must be set are the A and B controls, which describe the linearizer output relationship:

$$U_{eff} = A + BE \tag{14}$$

The value of A in Eqn. (14) corresponds to the lower velocity of the linearized range (the velocity at which the linearizer output voltage is zero), while the value of B corresponds to the range of linearization $(V_{maximum} - V_{minimum})$ divided by the output voltage range (10.0 volts).

The control potentiometers for A and B deal with normalized values of the coefficients A and B, calculated as follows:

Define

$$U^*_{eff} \triangleq A + B \times 10 \tag{15}$$

Then

$$\frac{U_{eff}}{U^*_{eff}} = \frac{A + BE}{A + B \times 10} \tag{16}$$

$$\frac{U_{eff}}{U^*_{eff}} = A^* + B^*E = \frac{A}{A+B\times 10} + \frac{B}{A+B\times 10}\,E \tag{17}$$

The values A^* and B^* are the control coefficients set into the Flow Analyzer. The values of A^* or B^* are assumed to be between 0.0 and 1.0

and are set into ten-turn potentiometers. The potentiometers are interrogated using a 10.0 volt reference voltage, supplied inside the Flow Analyzer, so that the value which appears at the test points is $10A^*$.

If

$$U_{eff,max} = 50 \tag{18}$$

$$U_{eff,min} = 20 \tag{19}$$

then

$$U_{eff} = 20 + 3.0\ E \tag{20}$$

and

$$U^*_{eff} = 50 \tag{21}$$

$$\frac{U_{eff}}{U^*_{eff}} = 0.4 + 0.6\ E \tag{22}$$

The settings on the A^* and B^* potentiometers would be 400 and 600, and the test point voltages would be 4.000 and 6.000, respectively.

There is only one control potentiometer for A^*, but there are three for B^*, one for each channel. All three must be set the same.

There is a toggle switch for the A^* control which is used only for calibrations over very wide ranges of velocities, where the A^* value would be too small for accurate adjustment. This switch raises the test point voltage by a factor of 10 for a given effective value of A^*.

There are nine potentiometers in the Jorgensen matrix. Each represents 1000 units, full scale, and can accept any value from 0.000 to 1000. A ten-volt reference, supplied from within, generates the test point voltages. The array generates the inverse Jorgensen matrix. All sign information is hard-wired: only magnitudes appear at the test points, thus all displayed voltages are positive.

The third elemental matrix results from the orthogonal wire geometry and does not depend upon pitch or roll. It is important to note that the wire coordinate system used in this report is left-handed, while the lab coordinate system is right-handed. Eqn. (26) is consistent with that set of definitions. If two right-handed sets were used, the signs of some of the terms in Eqn. (26) would change. The wire coordinate system was chosen so that the components X, Y, and Z were positive whenever the approaching velocity lay within the cone of the wires.

The M matrix coefficients correspond to the inverse of the Jorgensen matrix, and are related to the velocity components, as shown below.

$$\begin{bmatrix} X^2 \\ Y^2 \\ Z^2 \end{bmatrix} = \begin{bmatrix} k_{11}^2 & 1 & k_{21}^2 \\ k_{22}^2 & k_{12}^2 & 1 \\ 1 & k_{23}^2 & k_{13}^2 \end{bmatrix}^{-1} \begin{bmatrix} U_{eff_1}^2 \\ U_{eff_2}^2 \\ U_{eff_3}^2 \end{bmatrix} \qquad (23)$$

$$\begin{bmatrix} X^2 \\ Y^2 \\ Z^2 \end{bmatrix} \triangleq M \begin{bmatrix} U_{eff_1}^2 \\ U_{eff_2}^2 \\ U_{eff_3}^2 \end{bmatrix} \qquad (24)$$

When $k_1 = 0.15$ *and* $k_2 = 1.02$, *we have*

$$M = \begin{bmatrix} -0.5058 & 0.5155 & 0.4750 \\ 0.4750 & -0.5058 & 0.5155 \\ 0.5155 & 0.4750 & -0.5058 \end{bmatrix} \qquad (25)$$

The corresponding test point voltages would be 5.058, 5.155, 4.750, 4.750, 5.058, 5.155, 5.155, 4.750, and 5.058, respectively.

Setting the Control Potentiometers on the Coordinate Rotation Unit

The Coordinate Rotation Unit (CRU) contains nine control potentiometers, each equipped with a polarity switch. The potentiometers represent 1000 units full scale, and are interrogated with a 10-volt positive reference signal.

Polarity is assigned with the toggle switch, magnitude by the adjustment of the potentiometers. Three master control switches are used to switch from "set" to "run" positions. Potentimeter values cannot be assessed while in the "run" position: the voltages are meaningless.

The coefficients in the CRU are taken from the following set of matrix operations:

$$N = \begin{bmatrix} \cos\omega & 0 & -\sin\omega \\ 0 & 1 & 0 \\ \sin\omega & 0 & \cos\omega \end{bmatrix} \begin{bmatrix} 1 & 0 & 0 \\ 0 & \cos\alpha & \sin\alpha \\ 0 & -\sin\alpha & \cos\alpha \end{bmatrix} \begin{bmatrix} \sqrt{3}/3 & \sqrt{3}/3 & \sqrt{3}/3 \\ -\sqrt{6}/6 & -\sqrt{6}/6 & \sqrt{6}/3 \\ -\sqrt{2}/2 & \sqrt{2}/2 & 0 \end{bmatrix} \tag{26}$$

The angle of pitch, ω, is zero when the axis of the probe is in the x-direction, in laboratory coordinates, with the probe facing upstream. The angle ω lies in the plane parallel to the test surface (i.e., parallel to the x-z plane) and is defined as positive in the following figure.

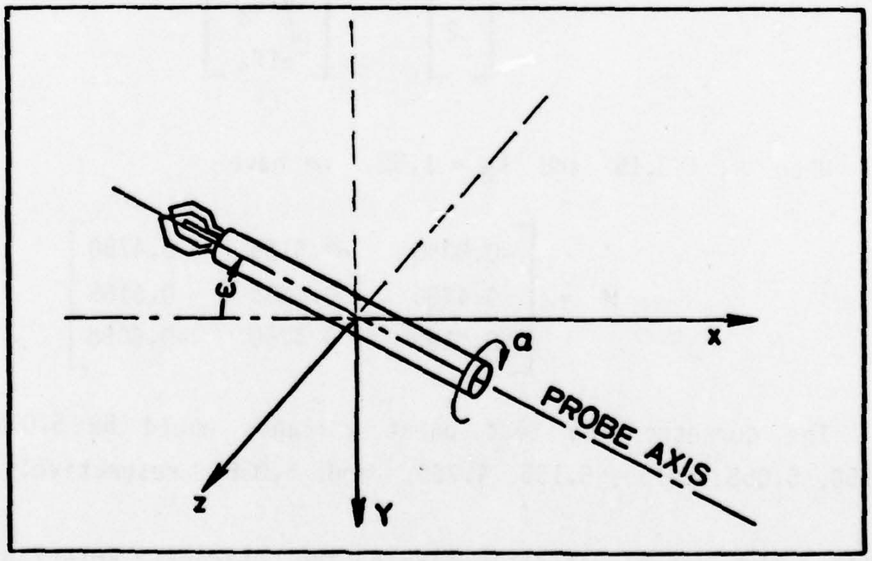

The angle of roll, α, is positive, as shown in the accompanying figure. The position of zero roll is defined to be the position in which wire #3 is in the x-y plane with the longer prong of wire #3 at the smaller y value.

In the calibration tsts reported here, the roll position of the probe was 90°. In this position, wire #3 is in the x-z plane, nearest to the test wall (an x-z plane).

The third elemental matrix results from the orthogonal wire geometry and is not a function of pitch or roll.

Interpretation of the Output Voltages

Voltages corresponding to the following velocity components are available at the panel of the Post Processor: $\overline{U}$, $\overline{V}$, $\overline{W}$, u',v',w', u'^2, v'^2, w'^2, $\overline{u'^2}$, $\overline{v'^2}$, $\overline{w'^2}$, $u'v'$, $u'w'$, $v'w'$, $\overline{u'v'}$, $\overline{u'w'}$, $\overline{v'w'}$, plus q^2 (i.e., $u'^2 + v'^2 + w'^2$) and $\overline{q^2}$.

These voltages are interpreted as velocities by multiplication by constant factors. In the following, E( ) refers to the value, in volts, displayed at the panel, and the leading coefficient, defined in terms of U^*_{eff}, is given.

$$\overline{U}, \overline{V}, \overline{W} = \frac{U^*_{eff}}{10} E(\overline{U},\overline{V},\overline{W})$$

$$u', v', w' = \frac{U^*_{eff}}{10} E(u',v',w')$$

$$u'^2, v'^2, w'^2 = \frac{U^{*2}_{eff}}{100} E(u'^2,v'^2,w'^2)$$

$$\overline{u'^2}, \overline{v'^2}, \overline{w'^2} = \frac{U^{*2}_{eff}}{100} E(\overline{u'^2},\overline{v'^2},\overline{w'^2})$$

Chapter IV

EXPERIMENTAL RESULTS

Developmental Testing on the Probe System

The results shown in Fig. 10 indicate the generation of spurious signals for $\overline{V}$ and $\overline{W}$, which increase as the pitch angle, ω, increases. The $\overline{W}$ signal is larger than the $\overline{V}$ signal, but both are of the same sign. The results in Fig. 10 were processed using only the Flow Analyzer and Coordinate Rotation Units; hence the spurious signals do not represent difficulties with the Post Processor.

Three possible causes for the spurious signals were recognized: (1) an actual disturbance of the flow field caused by the presence of the probe (i.e., the $\overline{V}$ and $\overline{W}$ components were real, though undesired), or (2) defects in the Flow Analyzer and Coordinate Rotation units which generated false outputs from good inputs, or (3) inadequacies in the Jorgensen directional matrix as applied to the present probes.

The conclusion, at present, is that the principal cause of the difficulty lies in the Jorgensen matrix or, at least, that the error signal is already present in the anemometer output signals. Supporting evidence for this position is presented in the following paragraphs.

The possibility that the spurious signals were reflecting an actual disturbance of the flow was investigated by a sequence of three tests: pitch displacement tests in the 2-D calibration channel, pitch displacement tests in a small-diameter free jet, and flow-visualization tests in the free jet. It was not possible to conduct a direct-flow visualization study in the 2-D channel, because of the construction of the tunnel. The free-jet system used for hot-wire calibration produced a jet of uniform velocity about 2 cm in diameter. The triple-wire probe was positioned in the jet so that only the prongs were in the high-velocity jet, not the probe stem, except at the highest pitch angle. Probe output was measured as a function of pitch angle, and compared with the results in the 2-D channel, where the entire probe is in the flow field. The results are shown in Fig. 26. The velocity in the 2-D channel was 10.91 m/s, while the jet calibrater was operated at 14.75 m/s. The response to pitch was the same in the two tests. Based on this similarity in responses, it was concluded that the 2-D channel flow and the jet flow behaved the same. With this established, smoke was injected into the jet flow and the flow field around the wires made visible. No signs of flow disturbance were found for low- and moderate-pitch angles.

A further point of interest in Fig. 26 is the apparent asymmetry of the pitch response. The aerodynamic axis of the probe seems to be about 0.5° to the negative pitch side of the apparent (optical) axis.

The second possibility was that the Flow Analyzer and Coordinate Rotation Unit were generating the spurious signals even though the proper input signals were being received. This was investigated by constructing a computer code which duplicated the processing steps of the Flow Analyzer and Coordinate Rotation Unit. With the same input values to the analog processor and to the computer simulation, the same outputs were recovered, within 1 or 2%: both giving evidence of the spurious $\overline{V}$ and $\overline{W}$ values. Based on this test, it was concluded that the analog system was performing correctly and that the difficulty was already present in the output signals from the linearizers.

The most likely candidates for the difficulty are the k_1 and k_2 coefficients, the directional sensitivity coefficients in the Jorgensen matrix. Single values of k_1 and k_2 are used, for each wire, but Jorgensen's data showed that both k_1 and k_2 were functions of Reynolds number and angle of incidence. The development of a better description of directional sensitivity is a high-priority future task for this program. At present, the spurious signals are accepted as limitations on the accuracy with which the flow direction and turbulence quantities can be measured.

Test Results on the Final Configuration

The final, fixed position triple-wire probe was built using the roll position $\alpha = +90^0$. This places the wire nearest the test wall parallel to the wall, with the other two wires symmetrically disposed about a line perpendicular to the wall, forming an equilateral triangle, looking downstream into the probe.

The probe was tested in the 2-D channel for mean velocity and fluctuation response, with all data being processed through the analog Post-Processor Unit.

The probe was calibrated in place, on the centerline of the channel, and the calibration of the system (anemometers and linearizers) was checked periodically throughout the data-acquisition period.

Figure 27 shows $\overline{U}$, $\overline{V}$, and $\overline{W}$ as functions of position across the channel for pitch positions of zero (aligned with the flow) and 20°. The $\overline{V}$ and $\overline{W}$ components reach a maximum of 2.4% of $\overline{U}$. As shown by the developmental tests, these are not the result of probe blockage affecting the flow, but are a consequence of inadequacies in the Jorgensen representation of directional sensitivity. The spurious $\overline{W}$ component observed at 20° pitch corresponds to an error in the apparent direction of flow of 1.4° only.

Figure 28 shows $\overline{u'v'}$ and $\overline{q^2}$ as a function of position across the channel, compared with the theoretical value based upon the pressure gradient within the channel. The measured shear stress lies within 2.5% of the true value for zero pitch and for 20° pitch. This should be compared with the values, shown in Fig. 11, where the Post Processor function was executed digitally. The improvement shown here reflects the simplified operating procedures, which resulted in less scatter in the linearizer signals.

Values of $\overline{u'^2}$, $\overline{v'^2}$, *and* $\overline{w'^2}$ *are* shown in Fig. 29, which should be compared with the data for zero pitch shown in Fig. 9.

Tests were also conducted at 30° pitch. The results showed that the magnitude of the mean velocity, $\overline{U}$, was read 1.4% high. The $\overline{W}$ value was nearly zero, less than 1%; hence the directional sensitivity is good, even near 30° pitch. The indicated shear stress was lower than the actual value by 30%.

Based on the above data, it appears that the useful range of the system can be described as follows:

- For mean velocity in the x-direction, $\overline{U}$, ±1.4%, up to pitch angles of 30°.
- For the direction of the mean velocity, within 1.5° for pitch angles up to 30° (1.5° error at 20° pitch was observed, 0° error at 30° pitch).
- For shear stress, within 2.5% for pitch angles up to 20°.

There are two contributors to the improved performance reported here compared with the original work: (1) the use of the gold-plated wires in the probe assembly, and (2) the improved operating procedure described in

Ch. IV. If it were important to assign the responsibility to only one cause, it would most likely be the change in operating procedure which caused the biggest improvement.

Measurements in a Curved Boundary Layer

The triple-wire system was installed in the outer wall of the Curvature Rig, an air tunnel designed for study of the heat transfer and hydrodynamic behavior of boundary layers on convex surfaces. The objective was to demonstrate that the Triple-Wire Processor has been reduced to practice and used in a practical measuring task.

The flow situation consists of an isothermal flow of air at 15 m/s, moving around a smooth surface of 45 cm radius. The confining channel has been tested and shown to hold the static pressure uniform in the direction of flow; i.e., there is no streamwise acceleration of the boundary layer. The flow is known to be two-dimensional.

The measuring station chosen was 45° around a turn at constant radius. The boundary layer entered the turn with a thickness of 40 mm, with normal boundary layer characteristics.

The effects of the curvature are particularly visible in the results for $\overline{U}$ and $\overline{u'v'}$. Fig. 30 shows $\overline{U}$ versus y, while Fig. 31 shows $\overline{u'v'}$ versus y. The active shear stress is confined to a layer very near the wall, as opposed to a normal flat-plate boundary layer. Fig. 32 shows the components of turbulence kinetic energy: $\overline{u'^2}$, $\overline{v'^2}$, and $\overline{w'^2}$.

Experience with the Triple-Wire Processor so far indicates that it provides a rapid and accurate method of acquiring turbulence data. Considering the measurement of a single quantity (i.e., $\overline{u'^2}$ or $\overline{U}$), approximately 60 seconds suffices to read and record, with a 33.3 second averaging time, even with single-point, hand data acquisition. The principal remaining problem is related to probe size: the commercial triple-wire probe is too large.

The Miniature Triple Wire

Figure 33 shows a miniature triple-wire probe, designated Design #1. The probe has only four prongs, instead of six, using the center pin as a common lead for all three channels. Electrical cross-talk tests showed that negligible cross-talk would be present if the resistance of the common leadwire were held to 0.0012 ohms or less.

The miniature design required a new directional matrix, a matter of calibration. It proved very difficult to manufacture, however, and is not regarded as a practical design.

Design #2, not shown, is the same as Design #1, except that the center pin extends farther forward, rather than being short. The wires form an orthogonal set whose apex is pointed upstream, so that the approaching flow is always exterior to the enclosed quadrant, instead of interior as in Design #1. This probe will be extremely simple to manufacture, and all future effort will be concentrated on it.

References

Delleur, J. W., 1966, "Flow Direction Measurement by Hot-Wire Anemometry," Journal A.S.C.E., Engineering Mechanics Division, Vol. 92, p. 45.

Hoffmeister, M., 1972, "Using a Single Hot-Wire Probe in Three-Dimensional Turbulent Flow Fields," DISA Information No. 13, May, 1972, pp. 26-28.

Johnston, J. P., 1970, "Measurements in a Three-Dimensional Turbulent Boundary Layer Induced by a Swept Forward-Facing Step," J. Fluid Mechanics, Vol. 42, Part 4, pp. 823-844.

Jorgensen, F. E., 1971, "Directional Sensitivity of Wire and Fiber Film Probes, An Experimental Study," DISA Information No. 11, May, 1971, pp. 31-37.

Mojola, O. O., 1974, "A Hot-Wire Method for Three-Dimensional Shear Flows," DISA Information No. 16, July 1974, pp. 11-14.

Moussa, Z. M., and Eskinazi, S., 1975, "Directional Mean Flow Measurements Using a Single Inclined Hot Wire," Physics of Fluids, Vol. 18, No. 3, pp. 298-305.

Yavuzkurt, S., "Full-Coverage Film Cooling: Three-Dimensional Measurements of Turbulence Structure and Predictions of Recovery Region Hydrodynamics," Ph.D. thesis, Stanford University, 1977.

Zimmerman, D. R., and Abbott, D. E., 1975, "An Experimental Investigation of a Three-Dimensional Turbulent Boundary Layer," Technical Report CFMTR-75-1, May, 1975.

Appendix A

ANALYSIS OF THE $\left[\frac{u'v'}{10}\right]$ CHANNEL

Let

$$u' = A \sin \omega_1 t \tag{1}$$

$$V' = B \sin(\omega_2 t + \alpha) \tag{2}$$

$$\frac{u'v'}{10} = \frac{AB}{10} \sin \omega_1 t \times \sin(\omega_2 + \alpha) \tag{3}$$

$$\overline{\left[\frac{u'v'}{10}\right]^2} = \left[\frac{AB}{10}\right]^2 \overline{\sin^2 \omega_1 t \times \sin^2(\omega_2 t + \alpha)}$$

$$\sqrt{\overline{\left[\frac{u'v'}{10}\right]^2}} \triangleq \mathrm{RMS}^*\left\{\frac{u'v'}{10}\right\} = \frac{AB}{10} \sqrt{\overline{\sin^2 \omega_1 t \quad \sin^2(m_2 t + \alpha)}} \tag{4}$$

Set

$$\begin{gathered} \omega_1 = \omega_2 = \omega \\ \alpha = 0 \end{gathered} \tag{5}$$

Equation (4) becomes

$$\mathrm{RMS}^*\left\{\frac{u'v'}{20}\right\} = \frac{AB}{10} \sqrt{\overline{\sin^4 \omega t}} \tag{6}$$

Since the time-averaging of a quantity $(\ )$ is defined by

$$\overline{(\ )} \triangleq \frac{1}{\theta_1} \int_0^{\theta_1} (\ )\, d\theta \tag{7}$$

we can easily show that

$$\overline{(\sin^4 \omega t)} = \frac{1}{\pi} \int_0^{\pi} \sin^4 \theta \, d\theta = \frac{3}{8} \tag{8}$$

and (4) becomes:

$$\mathrm{RMS}^* \left\{\frac{u'v'}{10}\right\} = \frac{AB}{20}\sqrt{3/2} = 0.061237\ AB \tag{9}$$

A and B are defined by Eqns. (1) and (2) and represent amplitudes. For a pure sine wave signal,

$$\mathrm{RMS}\{u'\} = A/\sqrt{2} \tag{10}$$

$$\mathrm{RMS}\{v'\} = B/\sqrt{2} \tag{11}$$

(10) and (9) into (8) yields:

$$\mathrm{RMS}^* \left\{\frac{u'v'}{10}\right\} = \frac{\mathrm{RMS}\{u'\}\ \mathrm{RMS}\{v'\}}{10}\sqrt{3/2} = 0.12247\ \mathrm{RMS}\{u'\}\ \mathrm{RMS}\{v'\} \tag{12}$$

Note: Equations (9) and (12) include the DC and AC level of the signal. RMS^* denotes the "true rms value" of the signal, i.e., when the signal includes a DC component. However, RMS (without star) denotes *only* the rms value of the signal, as measured by the TSI meter: root-mean-square value of an AC voltage only.

The TSI rms meter, Model 1076, used in this work is designed for measurements of the root-mean-square value of the AC component. In order to get the *normalizing parameters for the outputs of channel* $\left\{\frac{u'v'}{10}\right\}$ *one must first delete the DC level of the output.*

Fron (3) and (5) we can write:

$$\left[\frac{u'v'}{10}\right] = \frac{AB}{10}\sin^2 \omega t = \frac{AB}{10}\left[\frac{1 - \cos 2\omega t}{2}\right] \tag{13}$$

$$\left[\frac{u'v'}{10}\right] = \frac{AB}{20} - \frac{AB}{20}\cos 2\omega t = \left[\frac{u'v'}{10}\right]' + \overline{\left[\frac{u'v'}{10}\right]} \tag{14}$$

So:

$$\left[\frac{u'v'}{10}\right] = -\frac{AB}{20}\cos 2\omega t$$

yielding:

$$\mathrm{RMS}\left\{\frac{u'v'}{10}\right\} \triangleq \sqrt{\overline{\left[\frac{u'v'}{10}\right]'^{2}}} = \frac{AB}{40}\sqrt{2} = 0.03536\ AB \tag{15}$$

Combining (15) with (10) and (11), we get:

$$\mathrm{RMS}\left\{\frac{u'v'}{10}\right\} = \frac{\sqrt{2}}{20}\,\mathrm{RMS}\{u'\}\ \mathrm{RMS}\{v'\} = 0.0707\ \mathrm{RMS}\{u'\}\ \mathrm{RMS}\{v'\} \tag{16}$$

From (14), the combination of the two fluctuations values u' and v' generates an average value $\left[\overline{u'v'}/10\right]$ and a fluctuation value $\left[u'v'/10\right]'$. From (14):

$$\mathrm{DC}\left\{\frac{u'v'}{10}\right\} \triangleq \overline{\left[\frac{u'v'}{10}\right]} = \frac{AB}{20} = \frac{\mathrm{RMS}\{u'\} \times \mathrm{RMS}\{v'\}}{10} \tag{17}$$

Note that Eqns. (16) and (17) can be combined to yield Eqn. (9), which includes the DC component of the signal.

Let $\omega = \omega' + \overline{\omega}$ be any signal, since $\overline{\omega^2} = (\overline{\omega})^2 + \overline{(\omega')^2}$, because $\overline{\overline{\omega}\omega'} = 0$, we can easily show that

$$\mathrm{RMS}^{*}\{\omega\} \triangleq \sqrt{\overline{\omega^2}} = \sqrt{(\overline{\omega})^2 + \overline{\omega'^2}} \tag{18}$$

Now if, from Eqn. (14):

$$\overline{\omega} = \overline{\left[\frac{u'v'}{10}\right]} = \frac{AB}{20} \tag{19}$$

$$\omega' = \left[\frac{u'v'}{10}\right]' = -\frac{AB}{20}\cos 2\omega t \tag{20}$$

$$\mathrm{RMS}^{*}\left\{\frac{u'v'}{10}\right\} = \sqrt{\left(\frac{AB}{20}\right)^2 + \overline{\left(\frac{AB}{20}\cos 2\omega t\right)^2}} = \frac{AB}{20}\sqrt{3.2} \tag{21}$$

and this is the same as Eqn. (9).

Appendix B

TIME AVERAGE OF A SIGNAL

$P(t)$ = signal which is a function of time

$$\text{time average: } \frac{1}{T}\int_0^T P(t)dt = \overline{P(t)}$$

Say PT) is a sine wave:

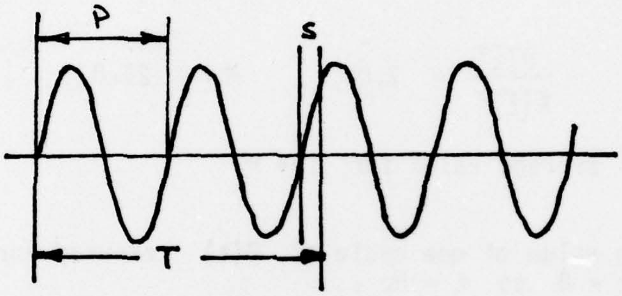

$T = Np + s$ = total time for integration

s = "scrap" time $= T - Np$

N = total number of periods in T

$$\overline{P(t)} = \frac{1}{T}\int_0^T P(t)\,dt$$

$$= \frac{1}{T}\left[\int_0^{Np} P(t)dt + \int_{Np}^{T} P(t)dt\right]$$

$$= \frac{1}{T}\left[\int_0^{Np} P(t)dt + \int_0^{s} P(t)dt\right]$$

$$= \frac{1}{T}\left[Np\,\overline{P(t)}' + s\,\widetilde{P(t)}'\right]$$

$$\overline{P(t)} = \frac{1}{Np+s}\left[Np\,\overline{P(t)}' + s\,\widetilde{P(t)}'\right]$$

for $Np >> s$

$$\overline{P(t)} = \overline{P(t)'}\left[1 + \frac{s}{NP}\,\frac{\widetilde{P(t)'}}{\overline{P(t)'}}\right]$$

for worst case: $s/p = 1/4$, and then:

$$\widetilde{P(t)} = \overline{P(t)'}$$

for rectified sine wave.

$$\overline{P(t)} = \overline{P(t)'}\left[1 + \frac{1}{4N}\right]$$

for

$$\frac{\overline{P(t)}}{\overline{P(t)'}} = 1.01 \quad , \qquad N = 25.0$$

$\overline{P(t)}$ = actual average value for $T = \infty$

$\overline{P(t)'}$ = average value of one cycle of $P(t)$ measured for a time increment from $t = 0$ to $t = Np$.

$\widetilde{P(t)}$ = average value of $P(t)$ measured from $t = Np$ to $t = Np + s$.

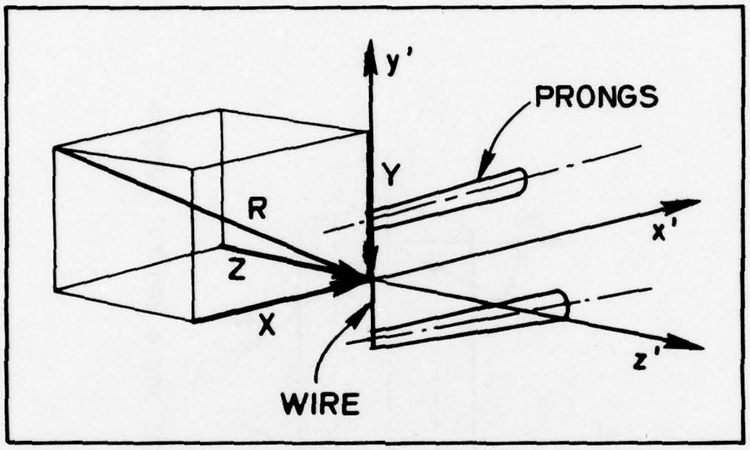

Fig. 1. Nomenclature for velocity components.

[illegible] Fig 1

from HMT-27, on III
Please return

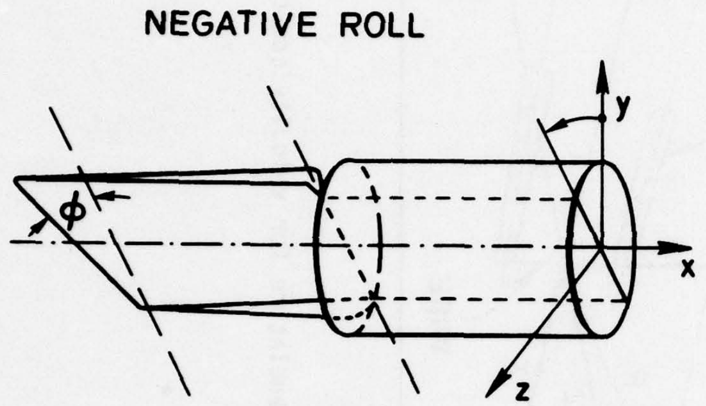

Fig. 2 Definition of slant angle and roll angle.

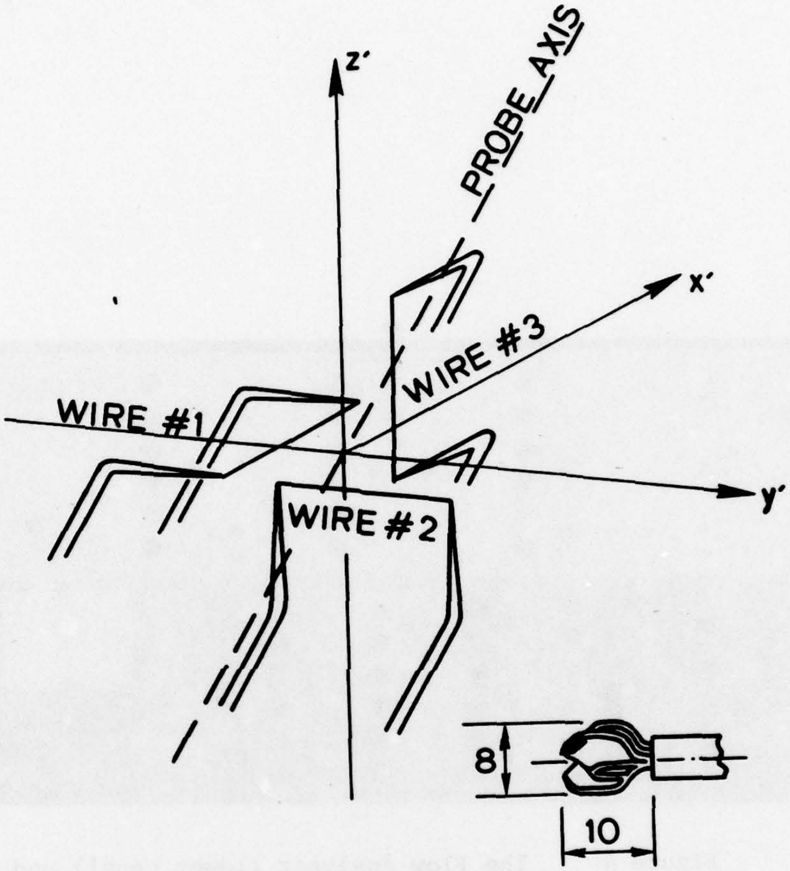

Fig. 3. Coordinate definition for the triple-wire probe.

FIG 3

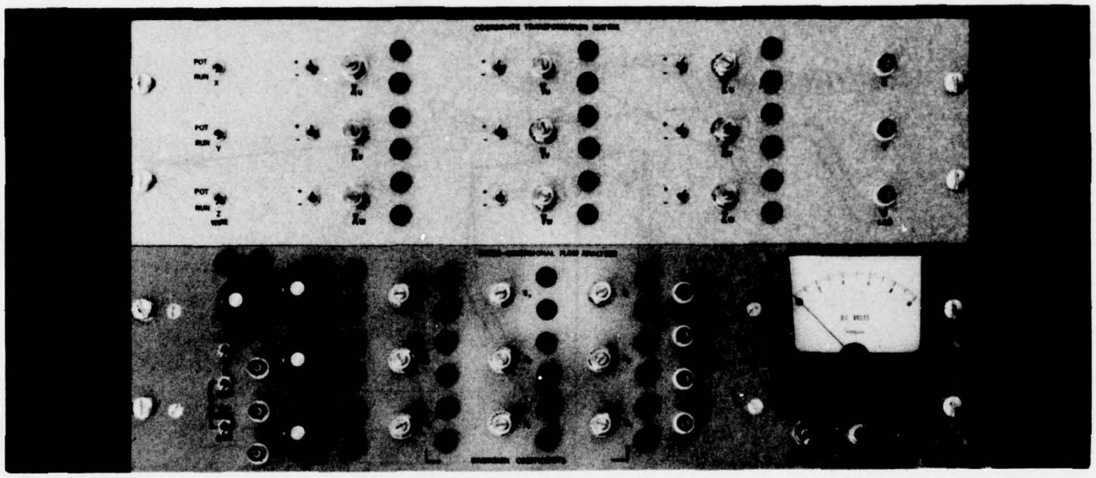

Figure 4 The Flow Analyser (lower panel) and Coordinate Rotation Unit

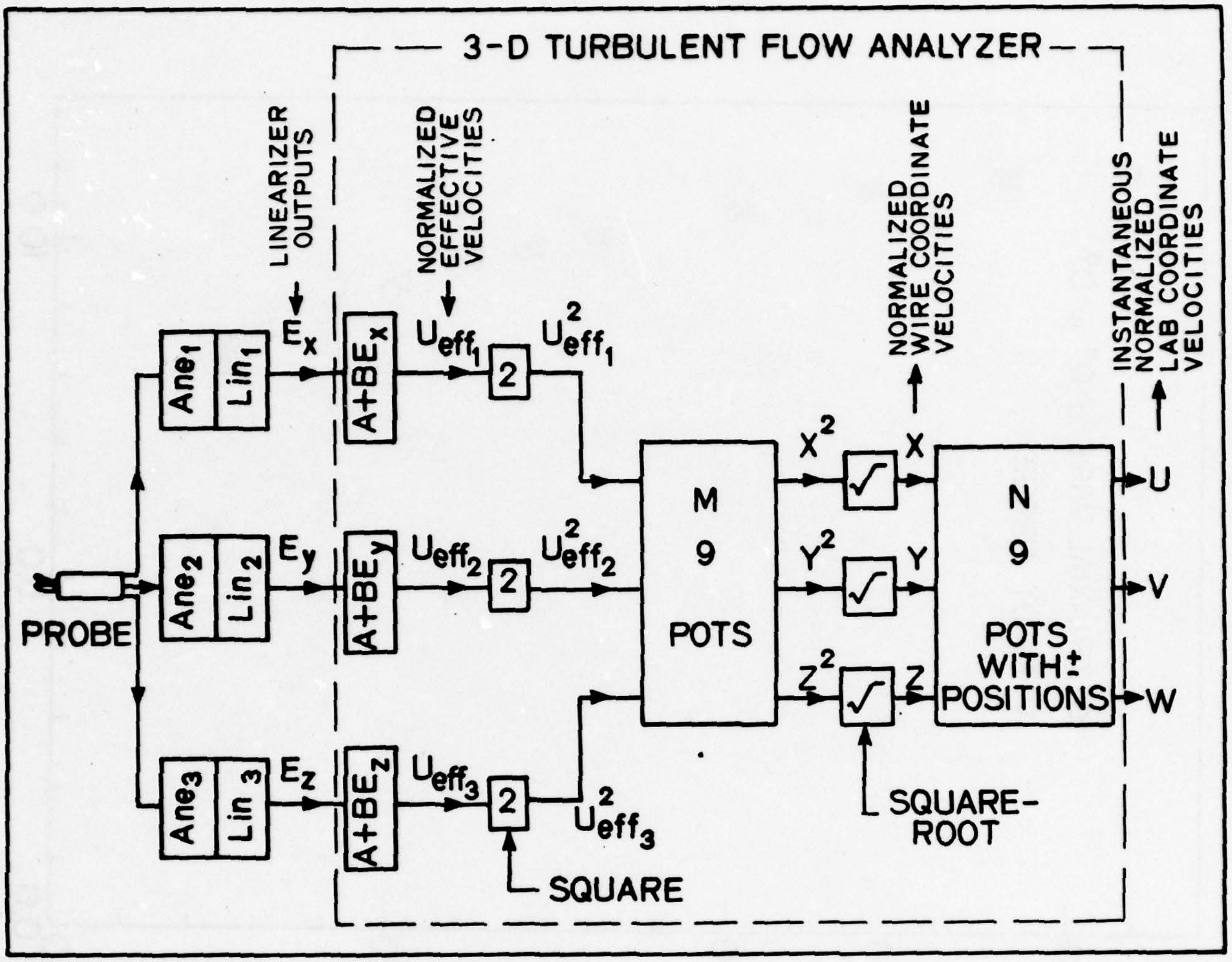

Fig. 5. Flow diagram of the Flow Analyzer and Coordinate Rotation Unit.

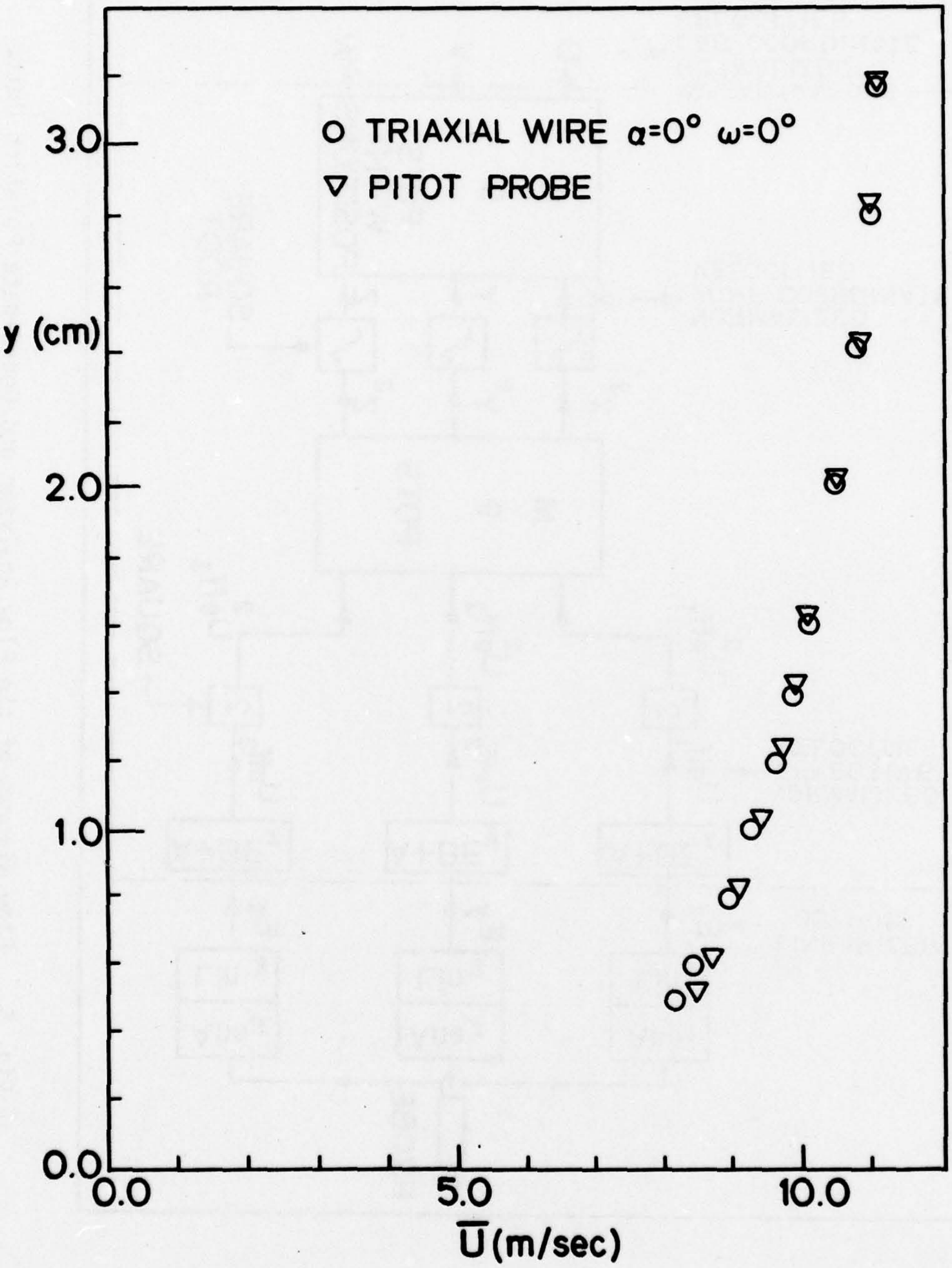

Fig. 6. Comparison of triple-wire and pitot-tube results.

Aug 79 [illegible]

[illegible]

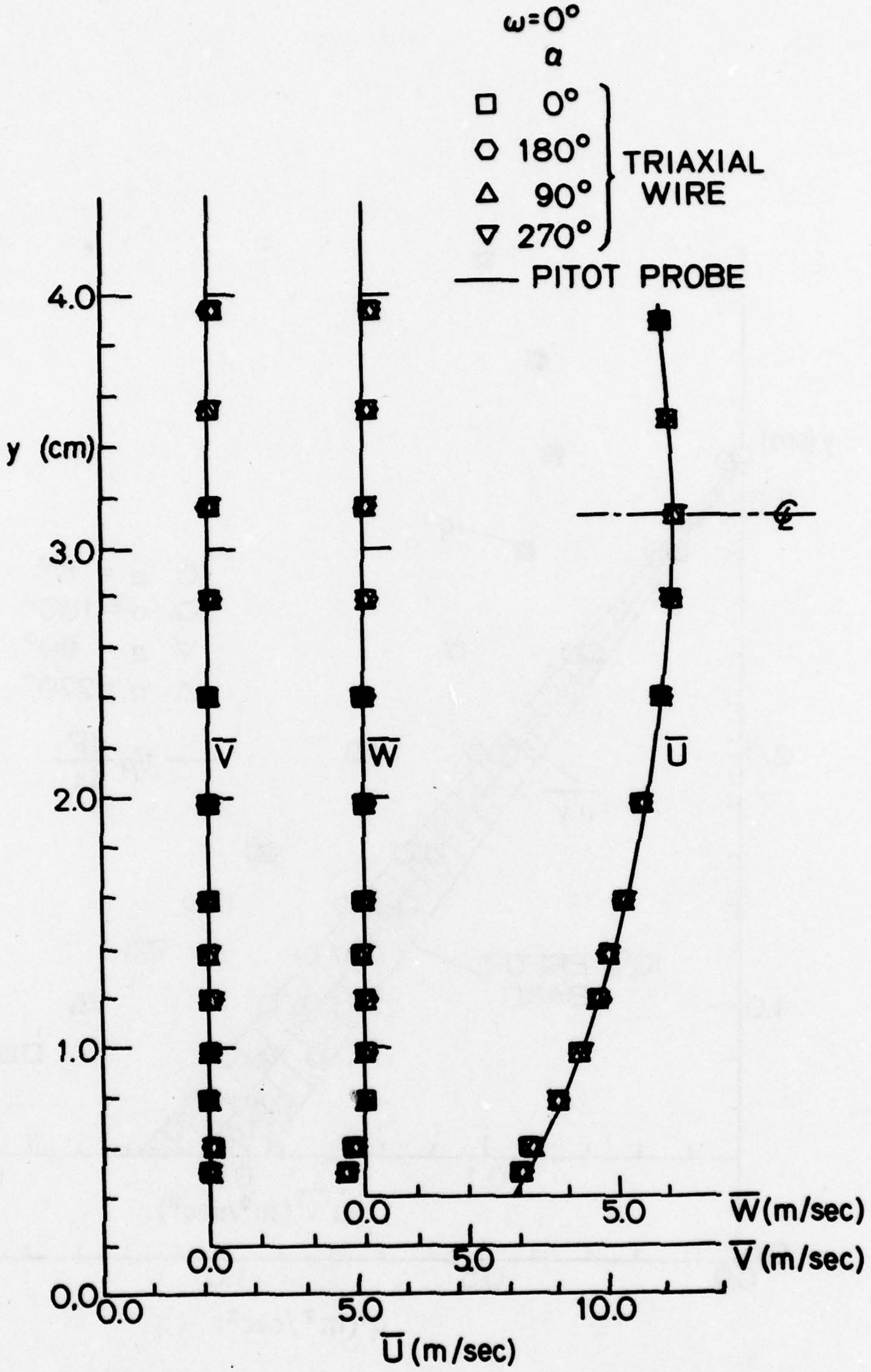

Fig. 7. Mean velocity components measured with different roll angles.

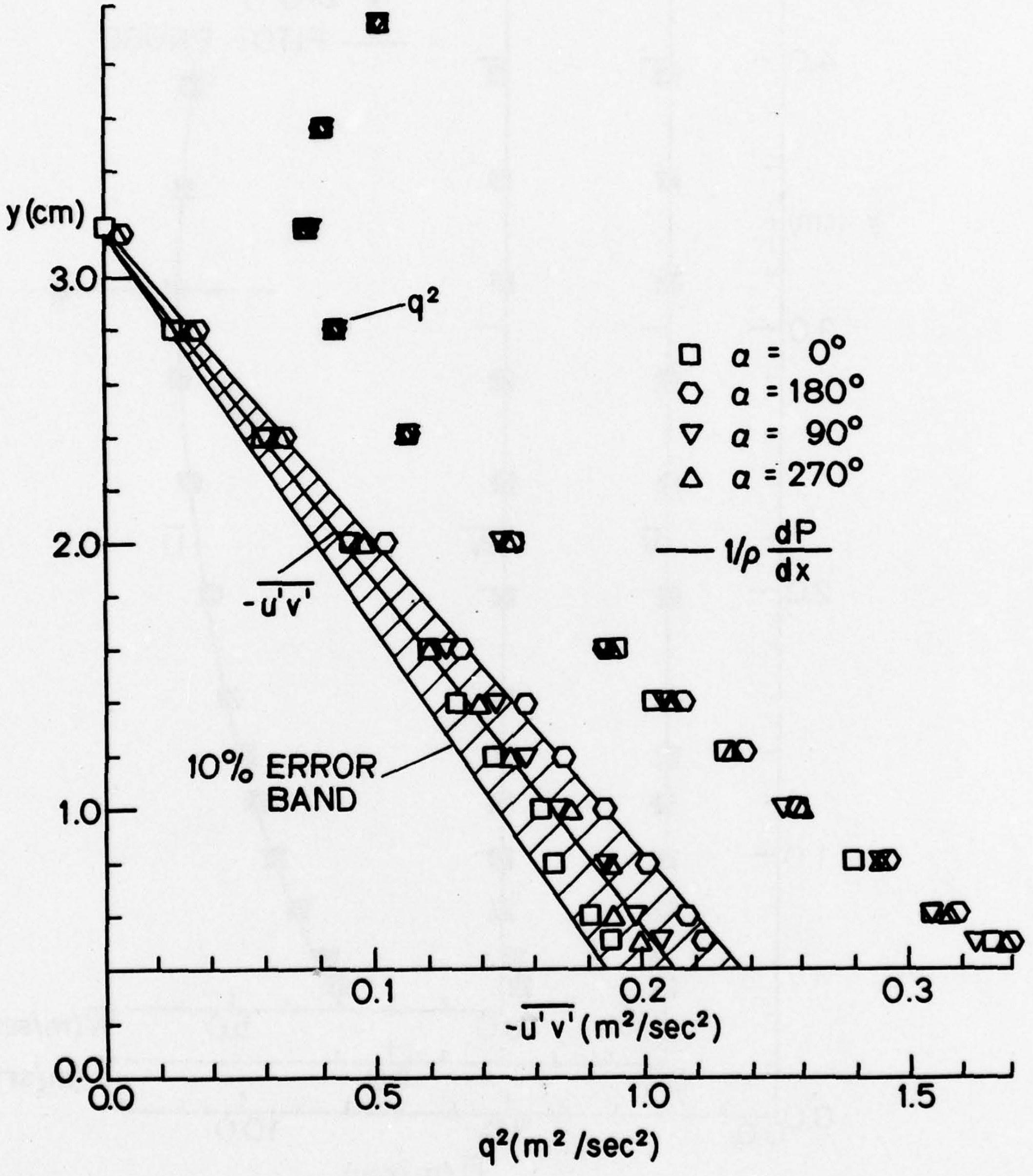

Fig. 8. Turbulent shear stress and turbulent kinetic energy measured with different roll angles, α.

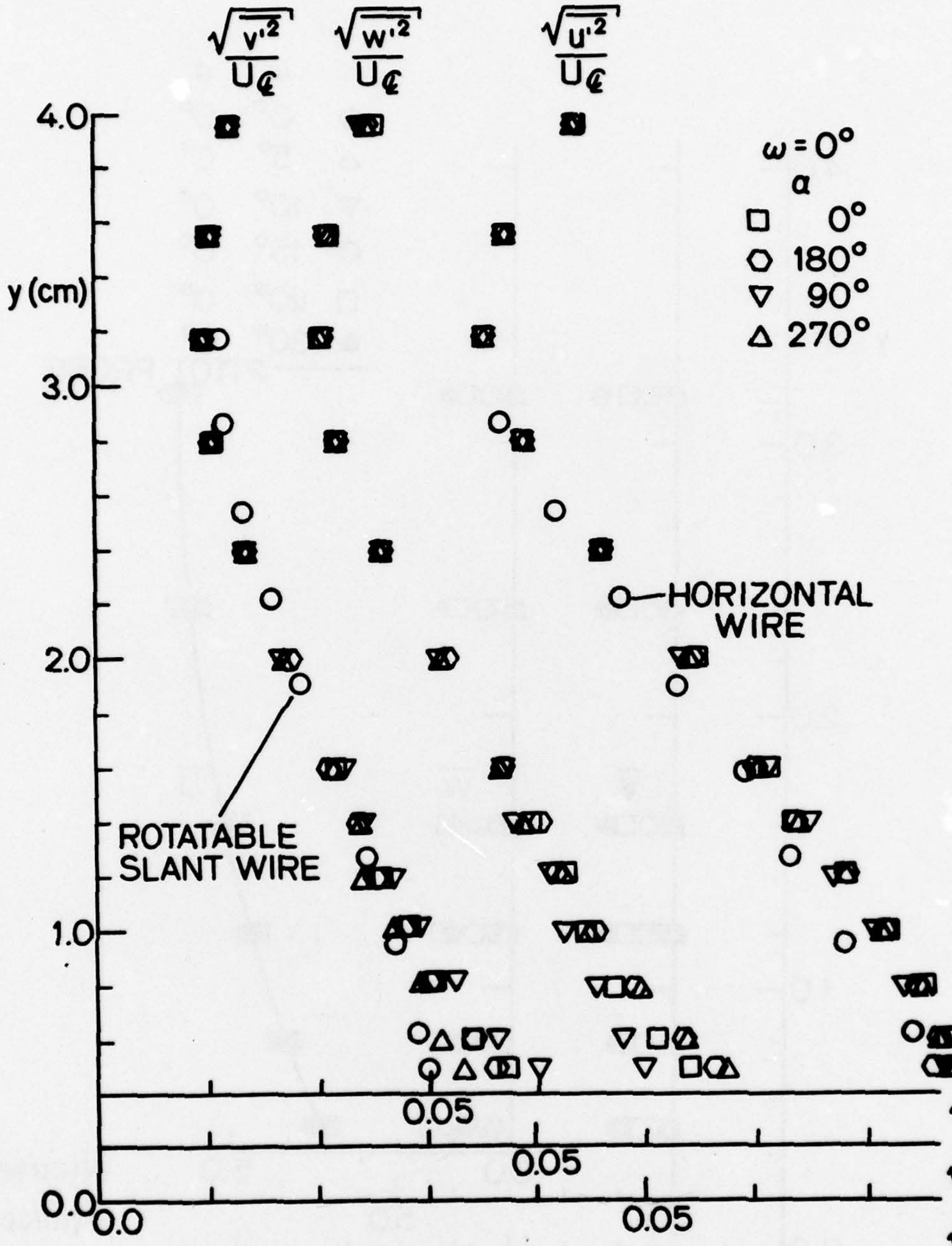

Fig. 9. The diagonal components of the reynolds stress tensor: $\overline{u'^2}$, $\overline{v'^2}$, and $\overline{w'^2}$.

Pg 7 [illegible]

Pt H[illegible]

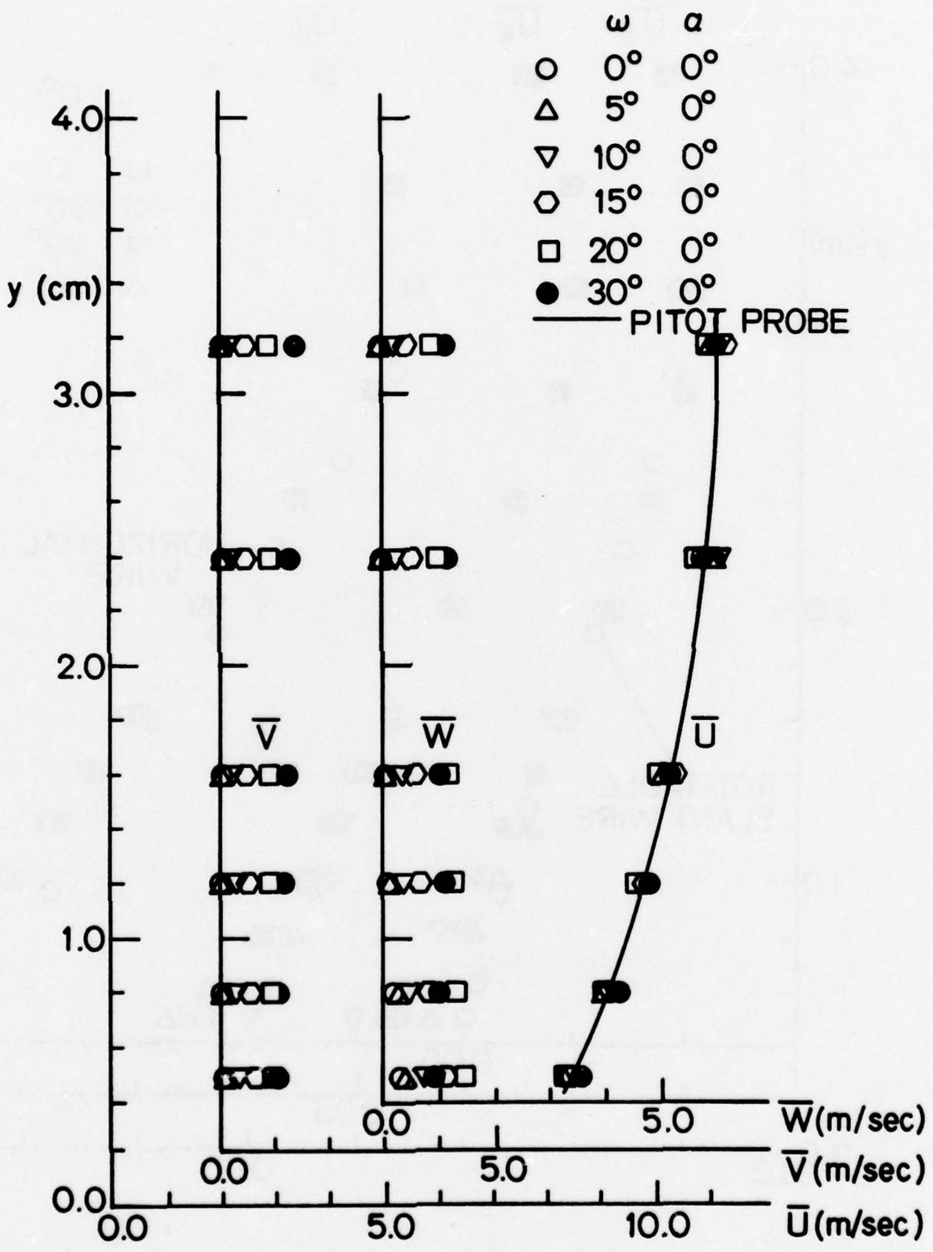

Fig. 10. Mean velocity components measured with different pitch angles, ω.

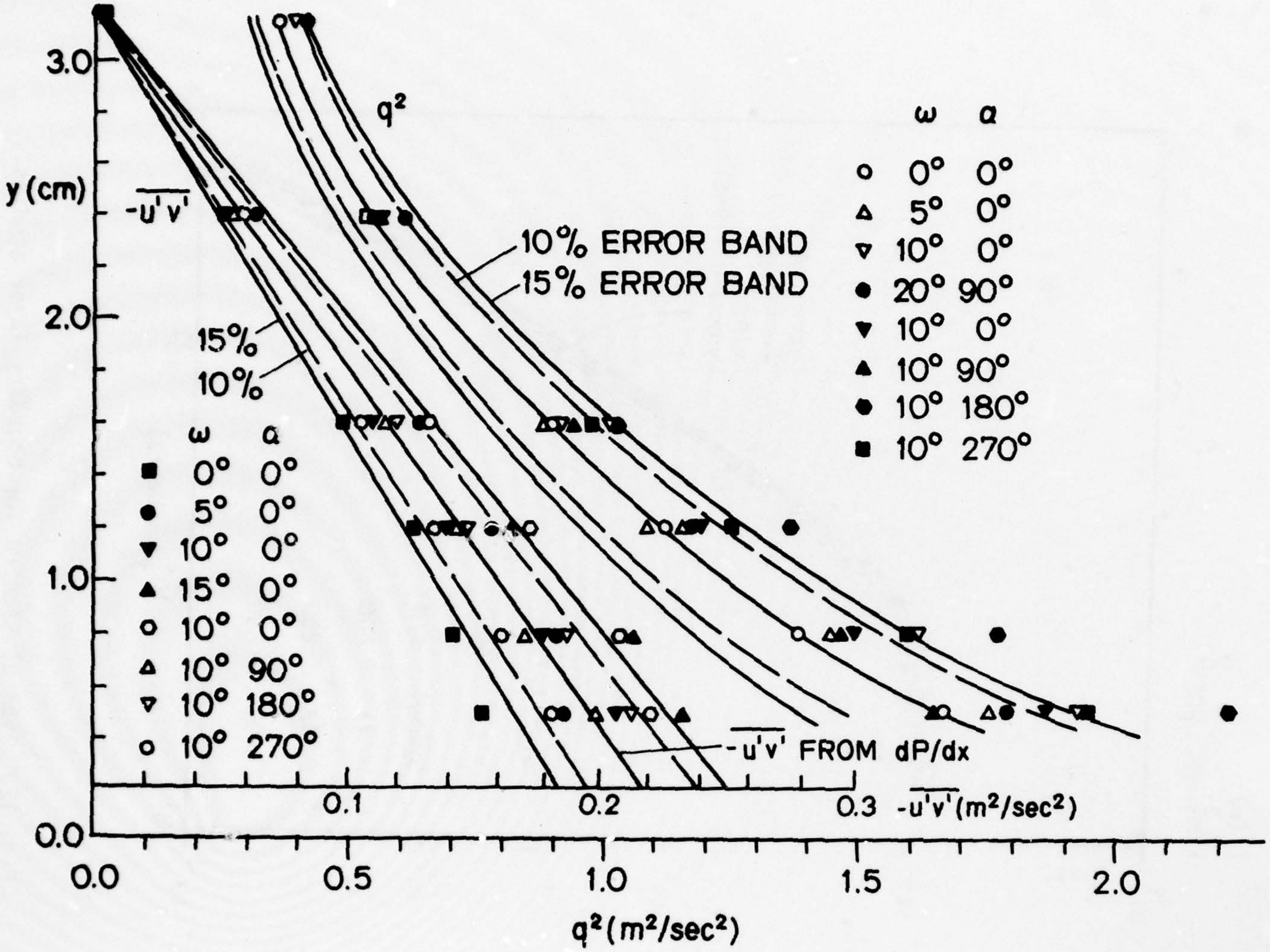

Fig. 11. Turbulence kinetic energy and shear stress for combined roll and pitch.

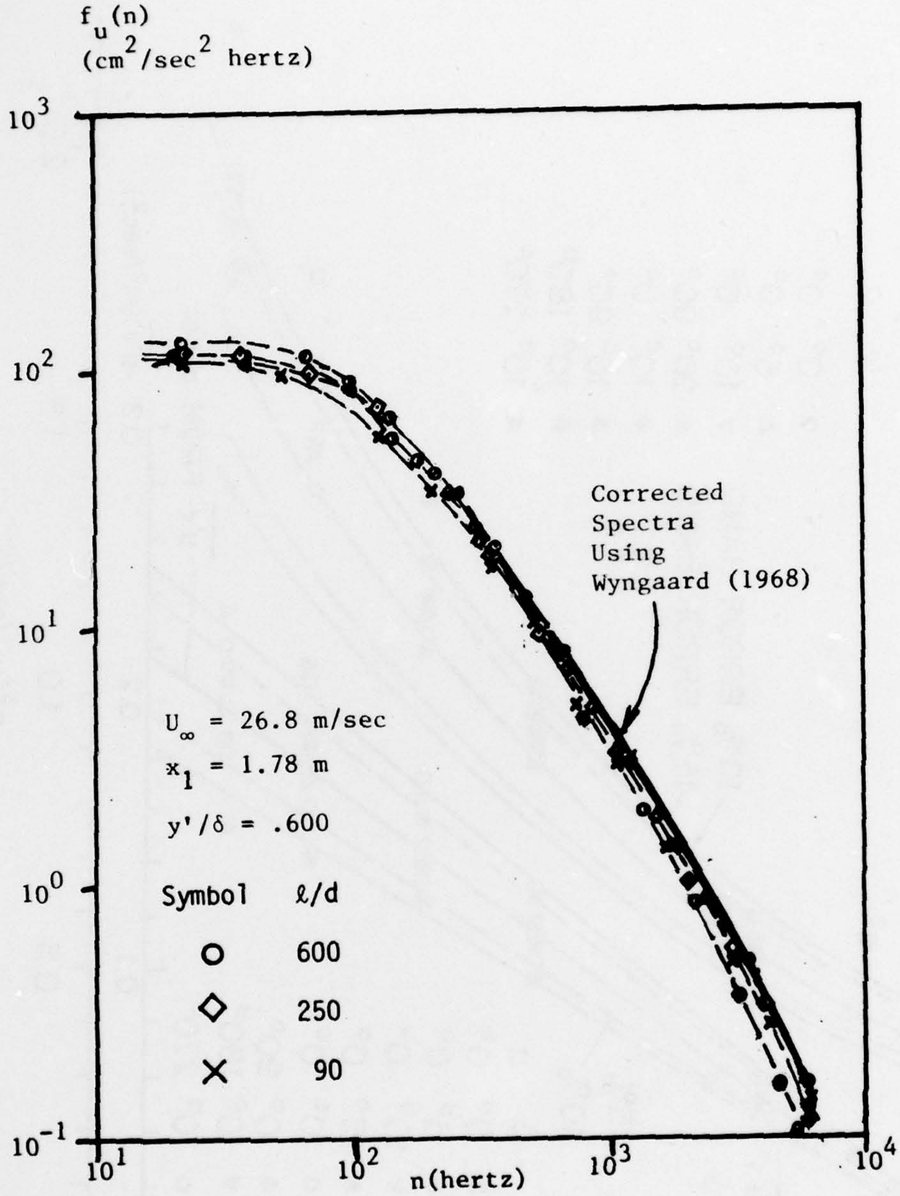

Fig. 12. Typical spectra for boundary layer studies.

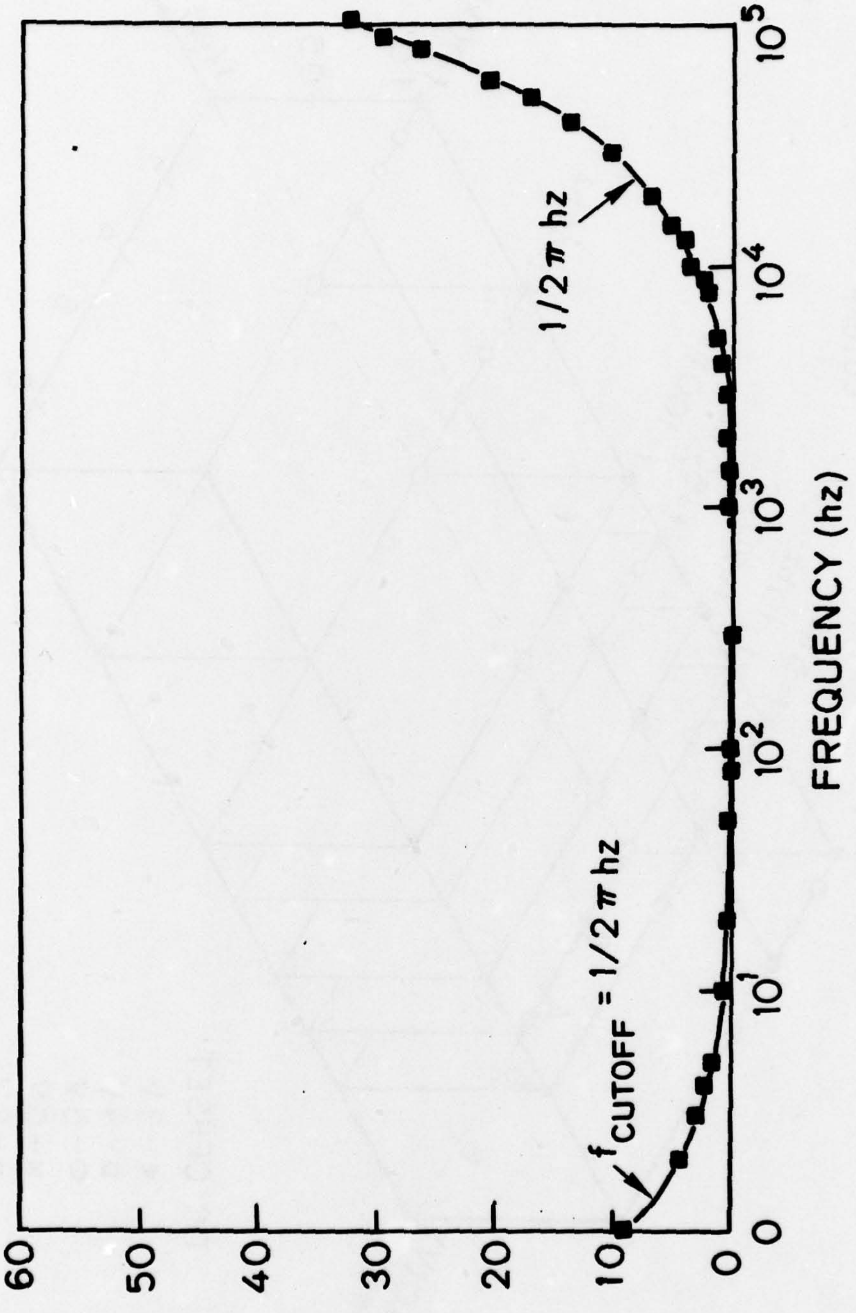

Fig. 13. The phase-shift characteristics of the low-pass filter.

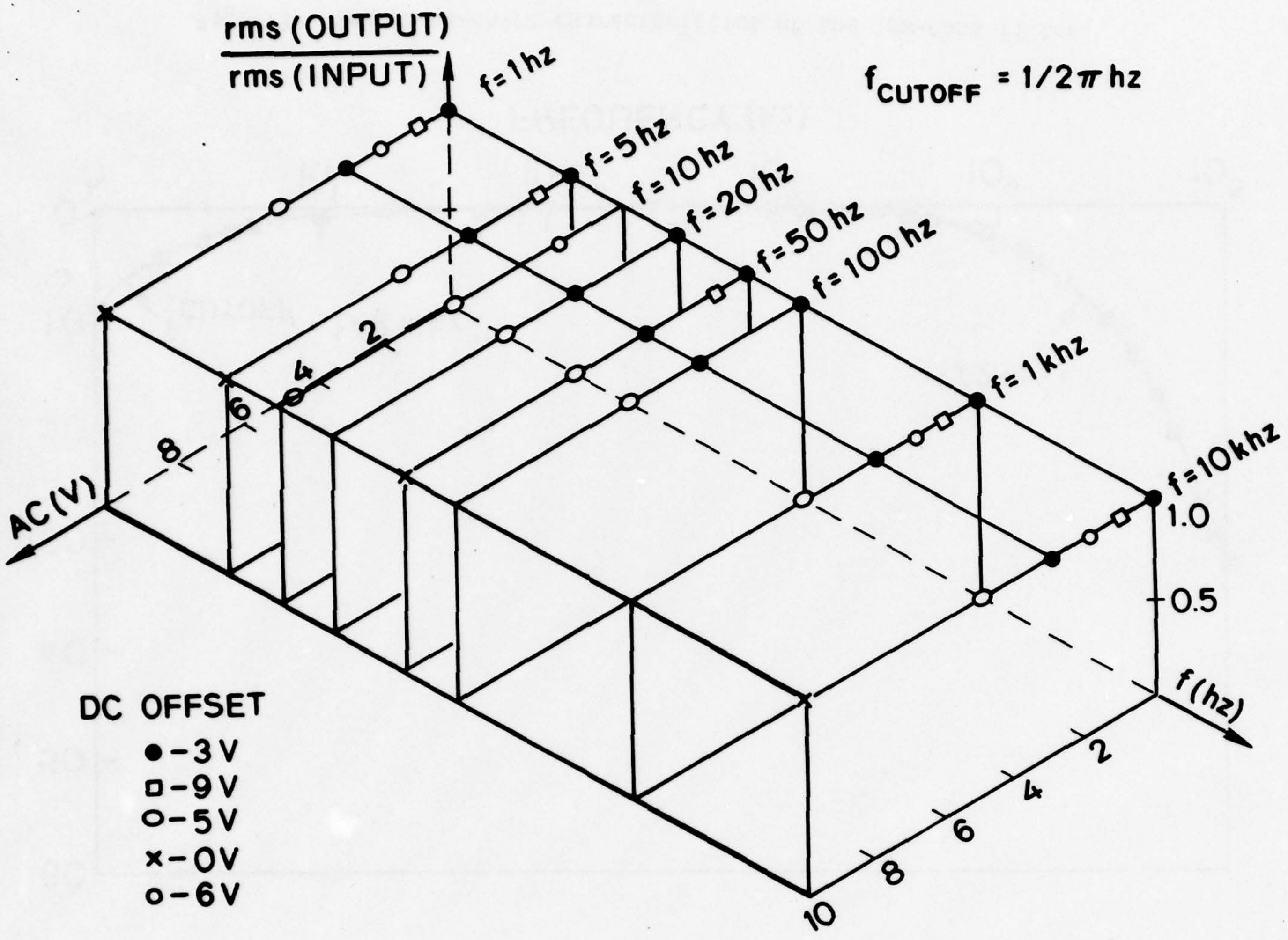

Fig. 14. The AC attenuation characteristics of the high-pass filter unit.

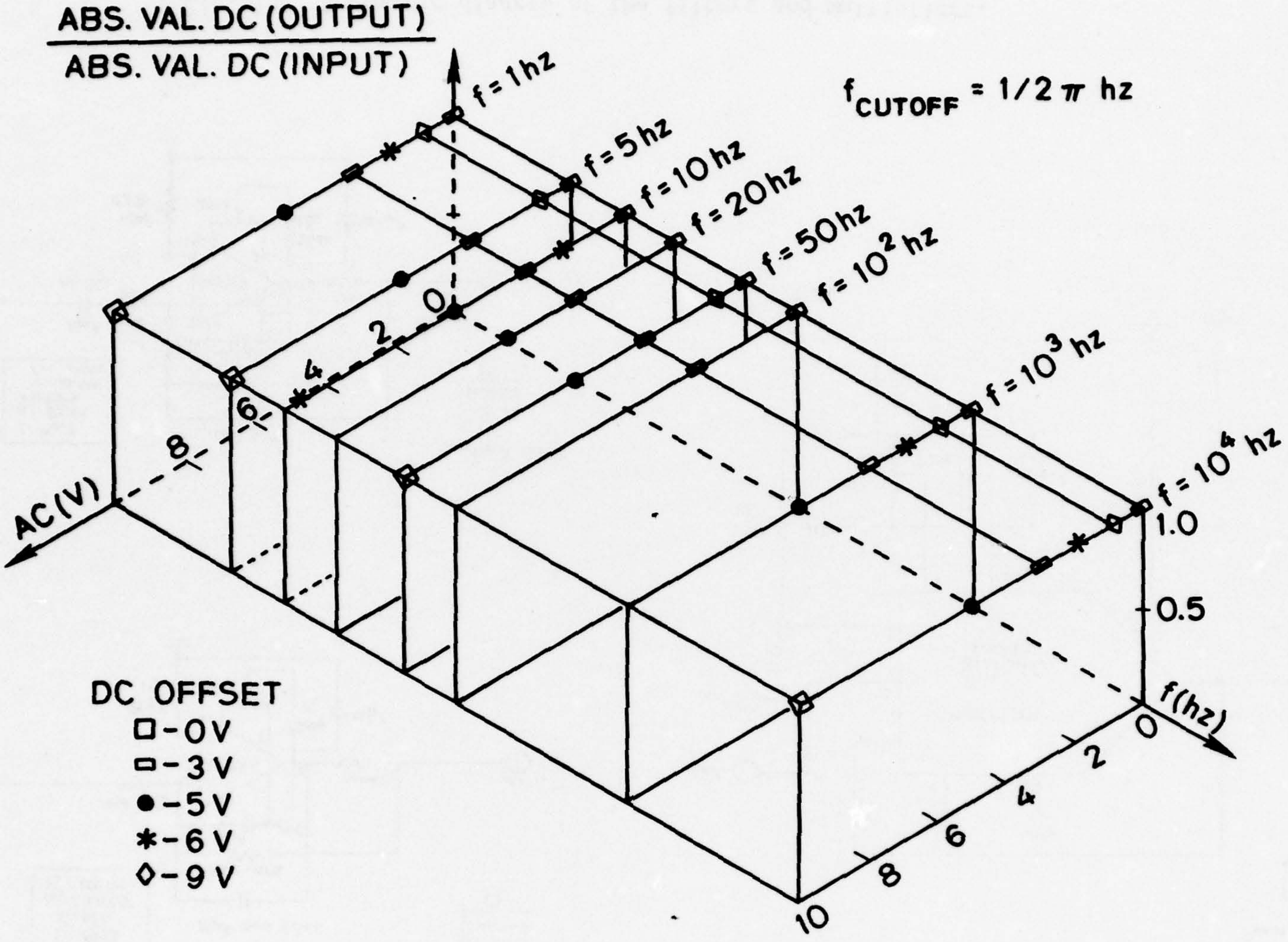

Fig. 15. The DC attenuation characteristics of the low-pass filter unit.

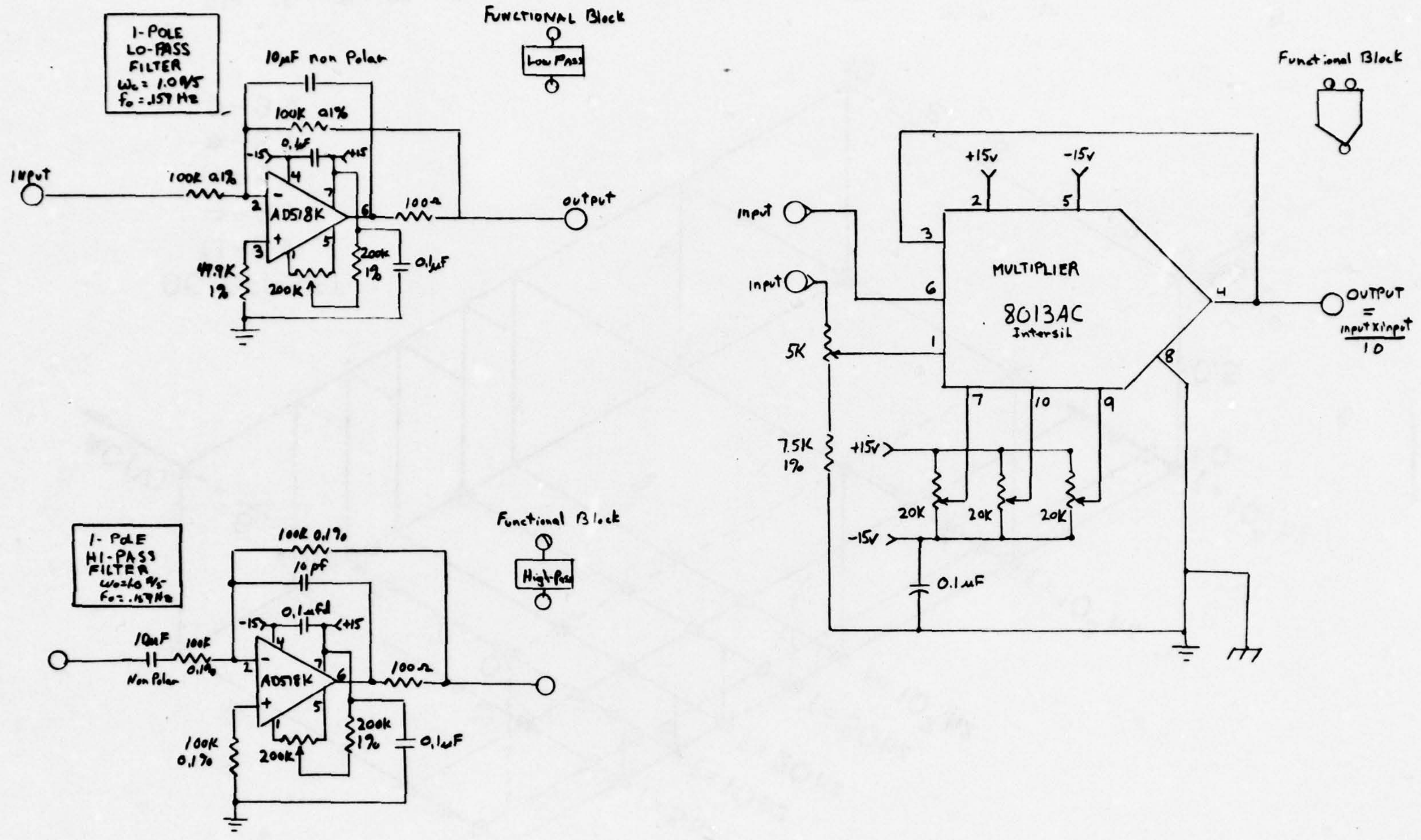

Fig. 16. Schematic diagram of the filters and multipliers.

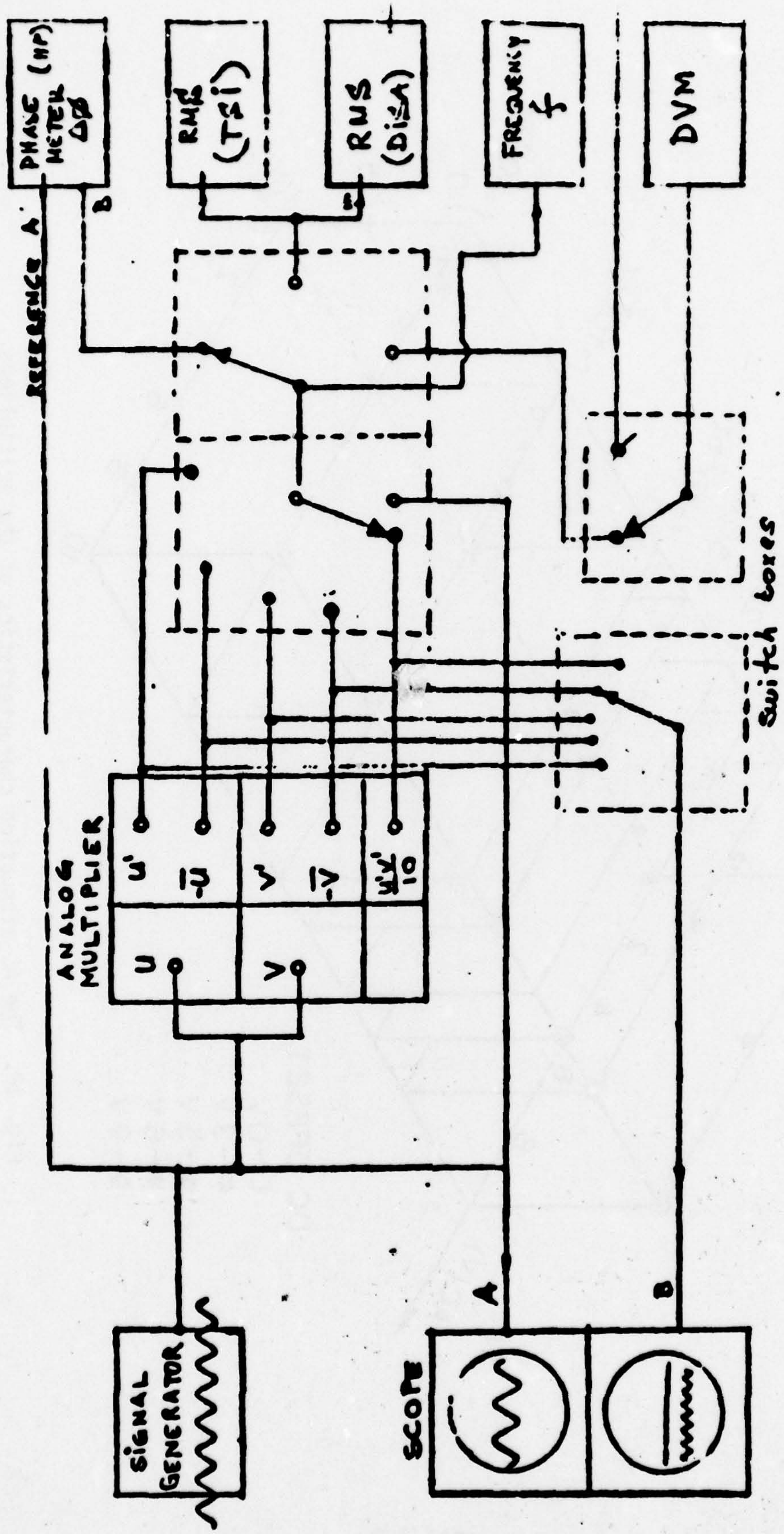

Fig. 17. Arrangement for testing the multipliers.

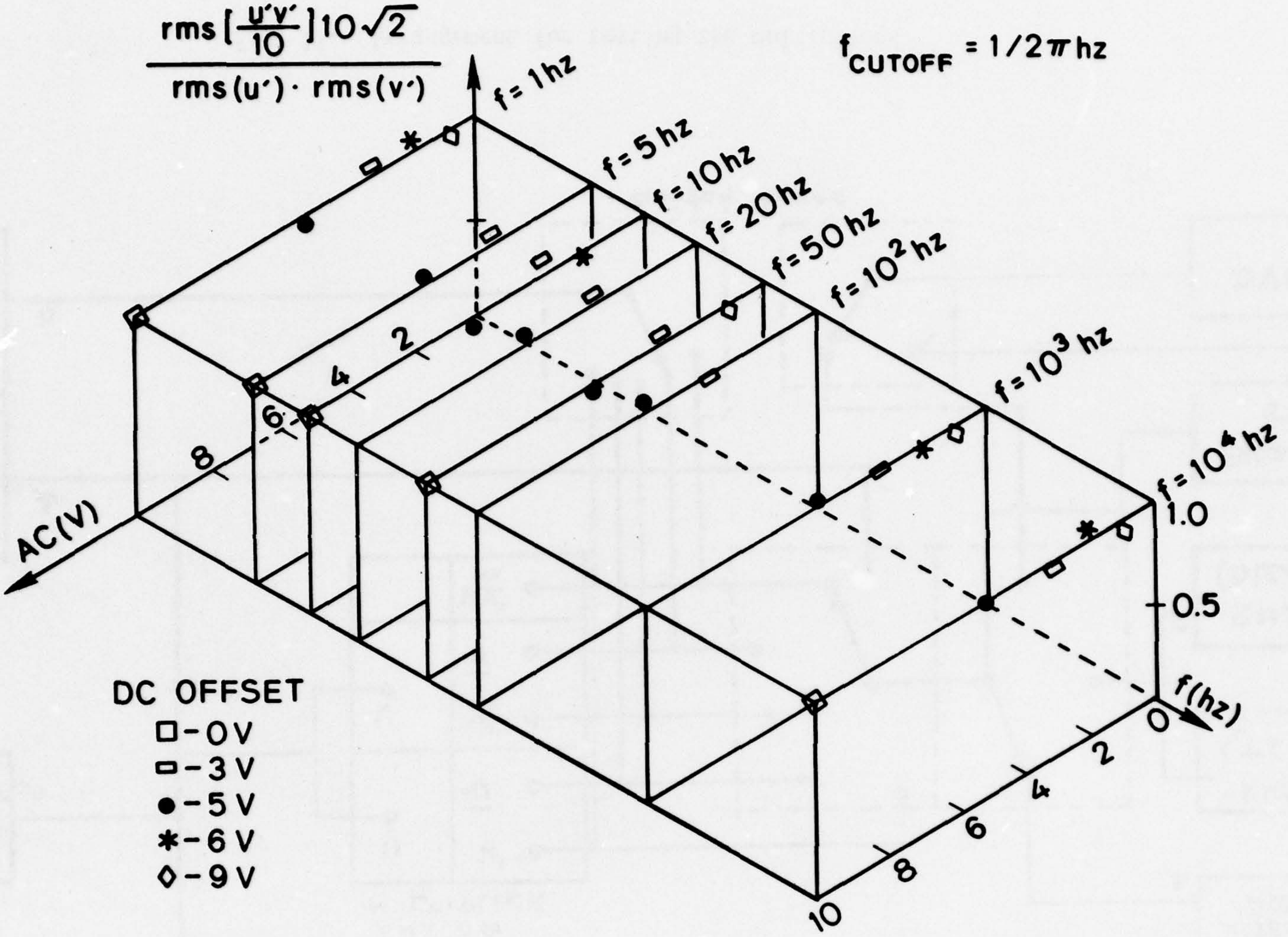

Fig. 18. The AC attnuation characteristics of the multipliers.

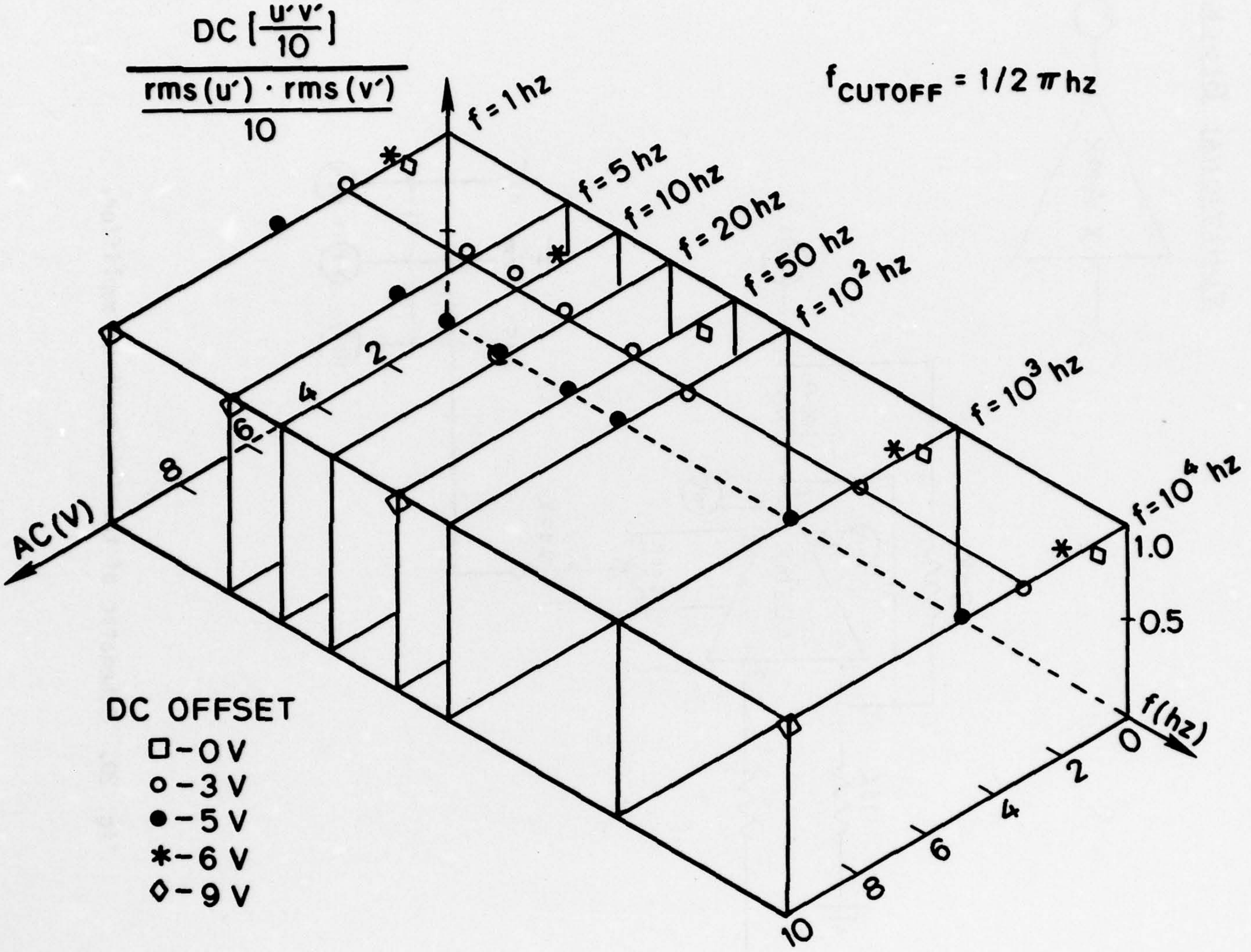

Fig. 19. The DC attenuation characteristics of the multipliers.

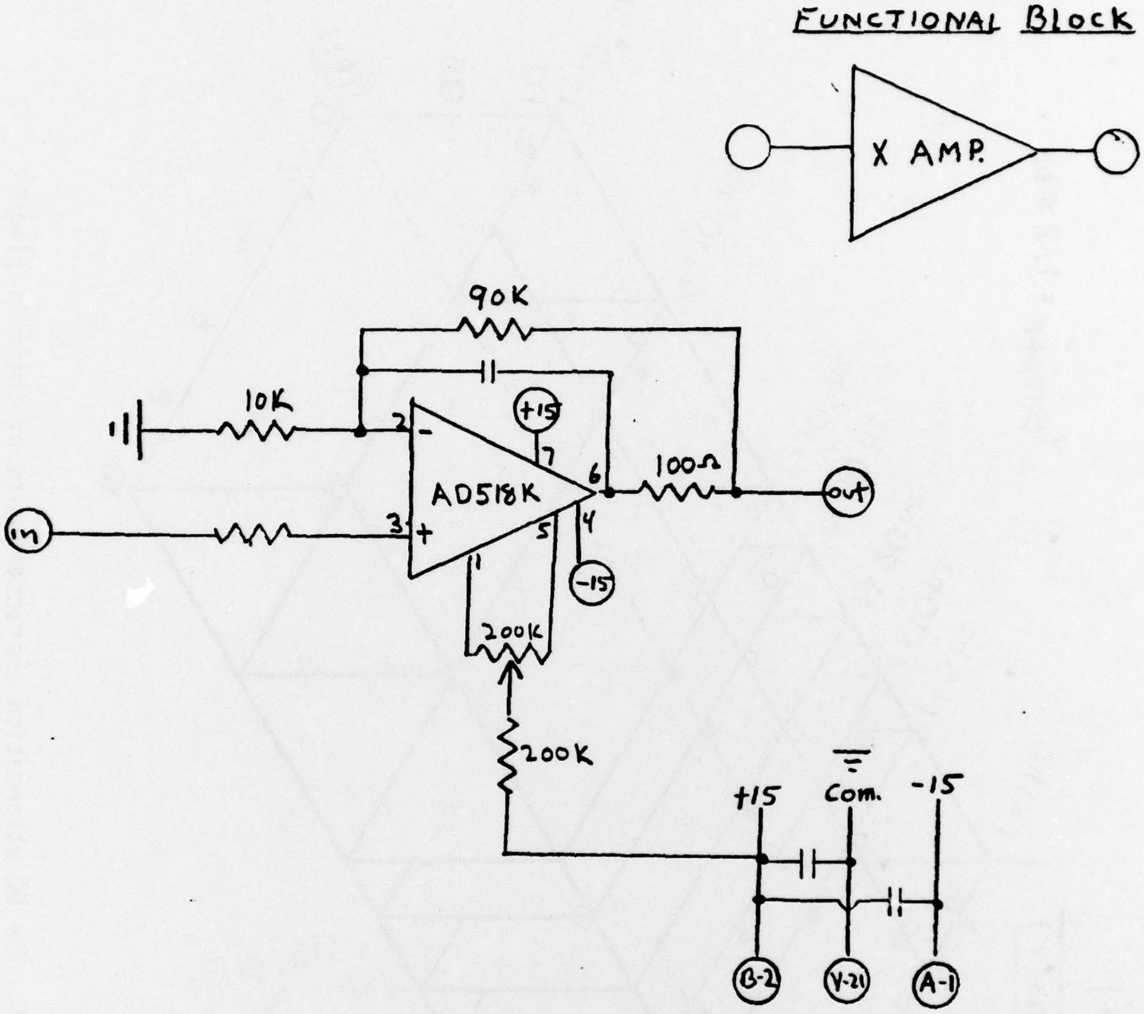

Fig. 20. Schematic of the intermediate amplifier.

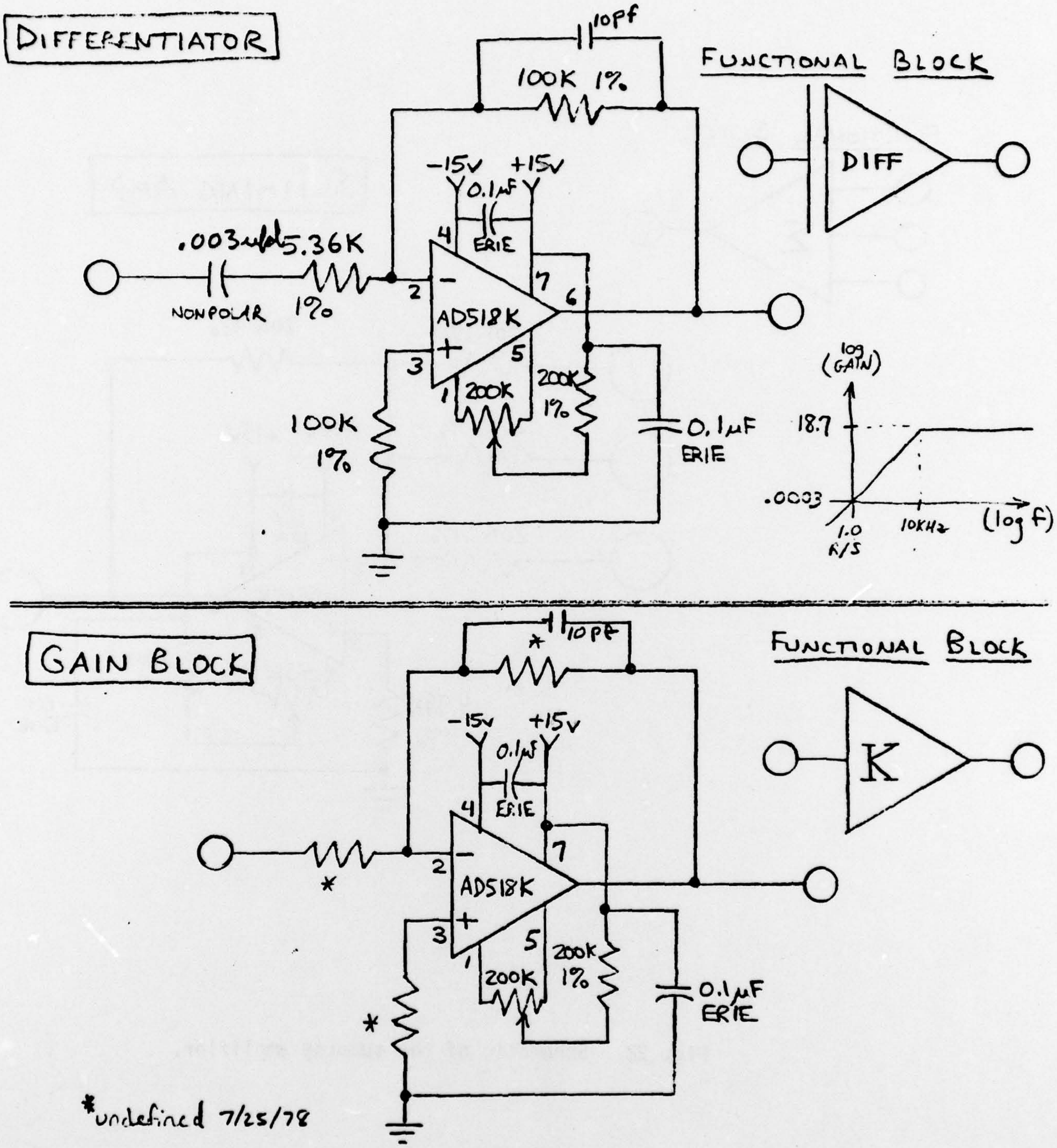

*undefined 7/25/78

Fig. 21. Schematic of the differentiator element and the gain block.

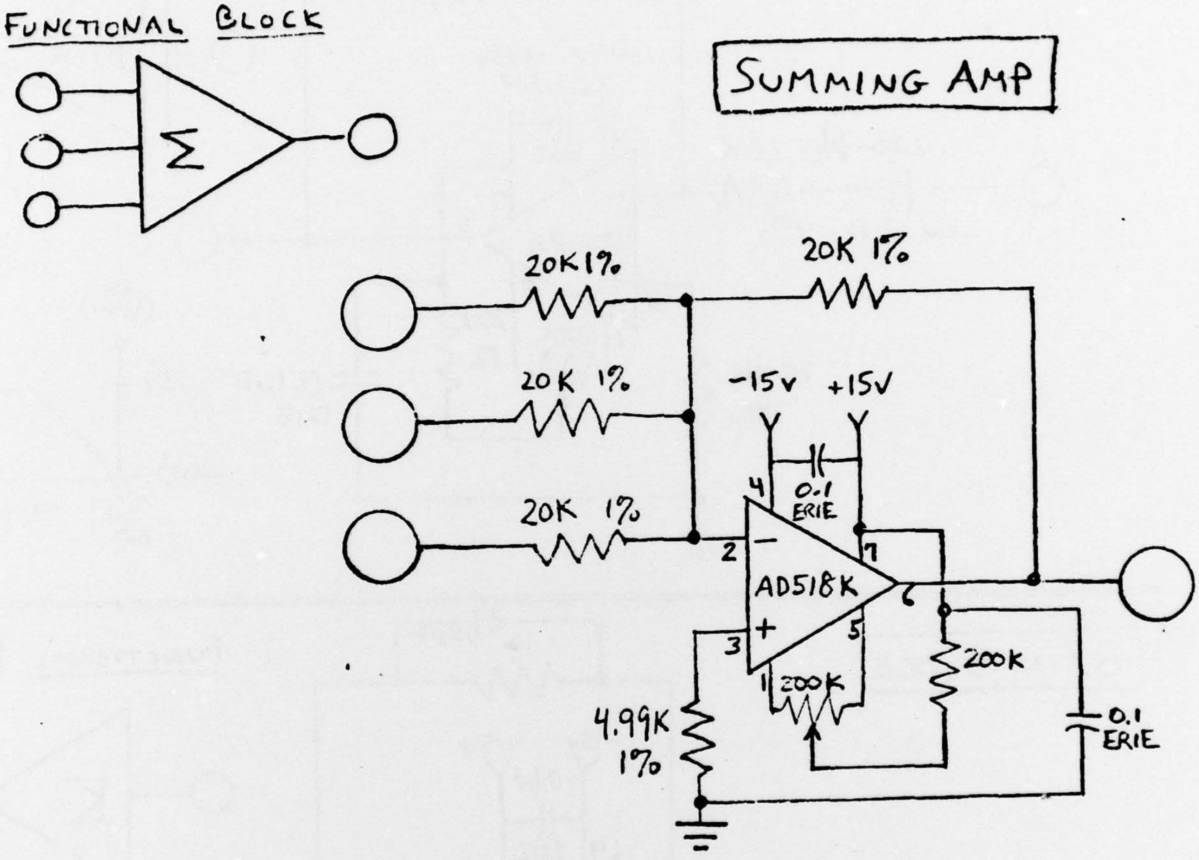

Fig. 22. Schematic of the summing amplifier.

22

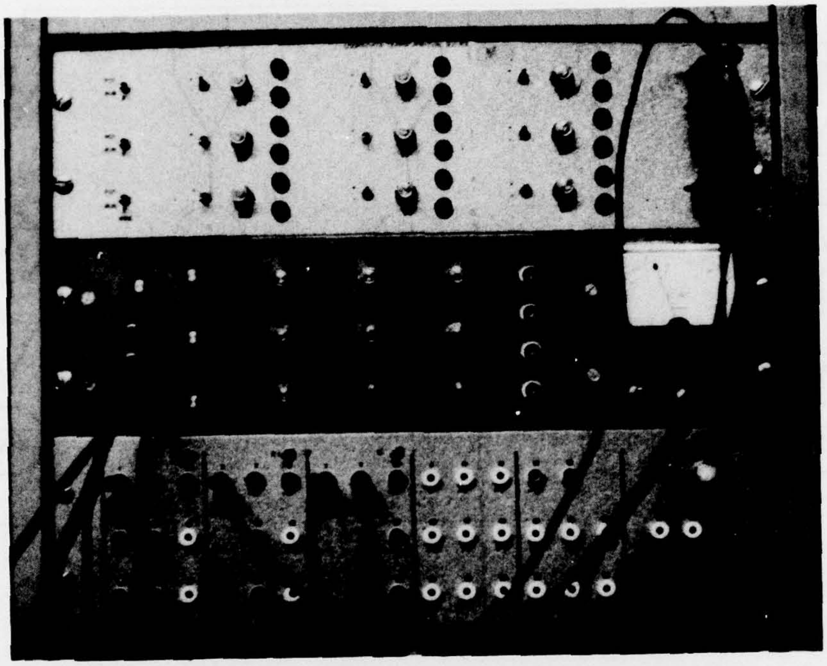

Figure 23 The Triple Wire Processor

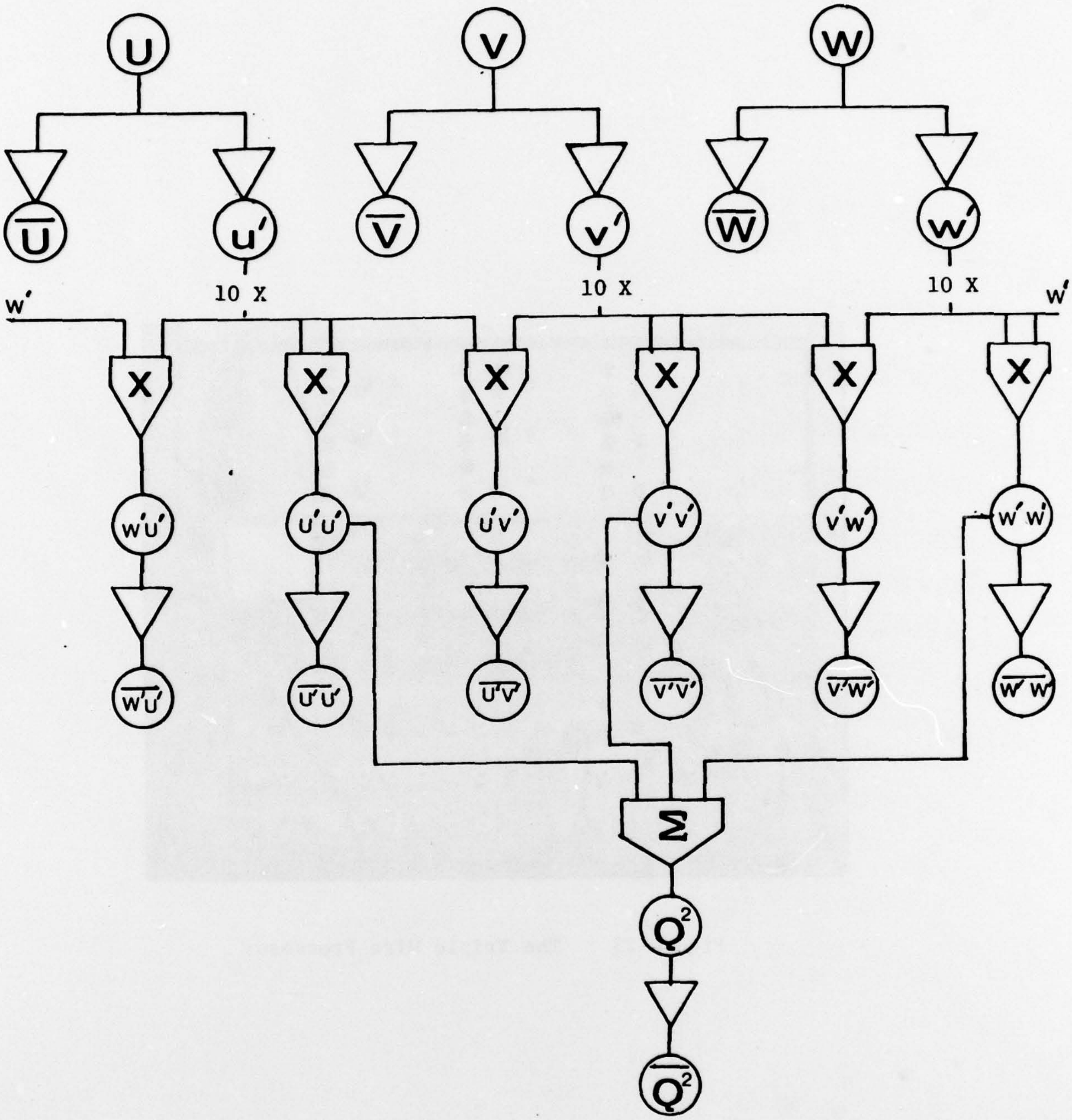

Fig. 24. Flow diagram of the Post Processor.

24

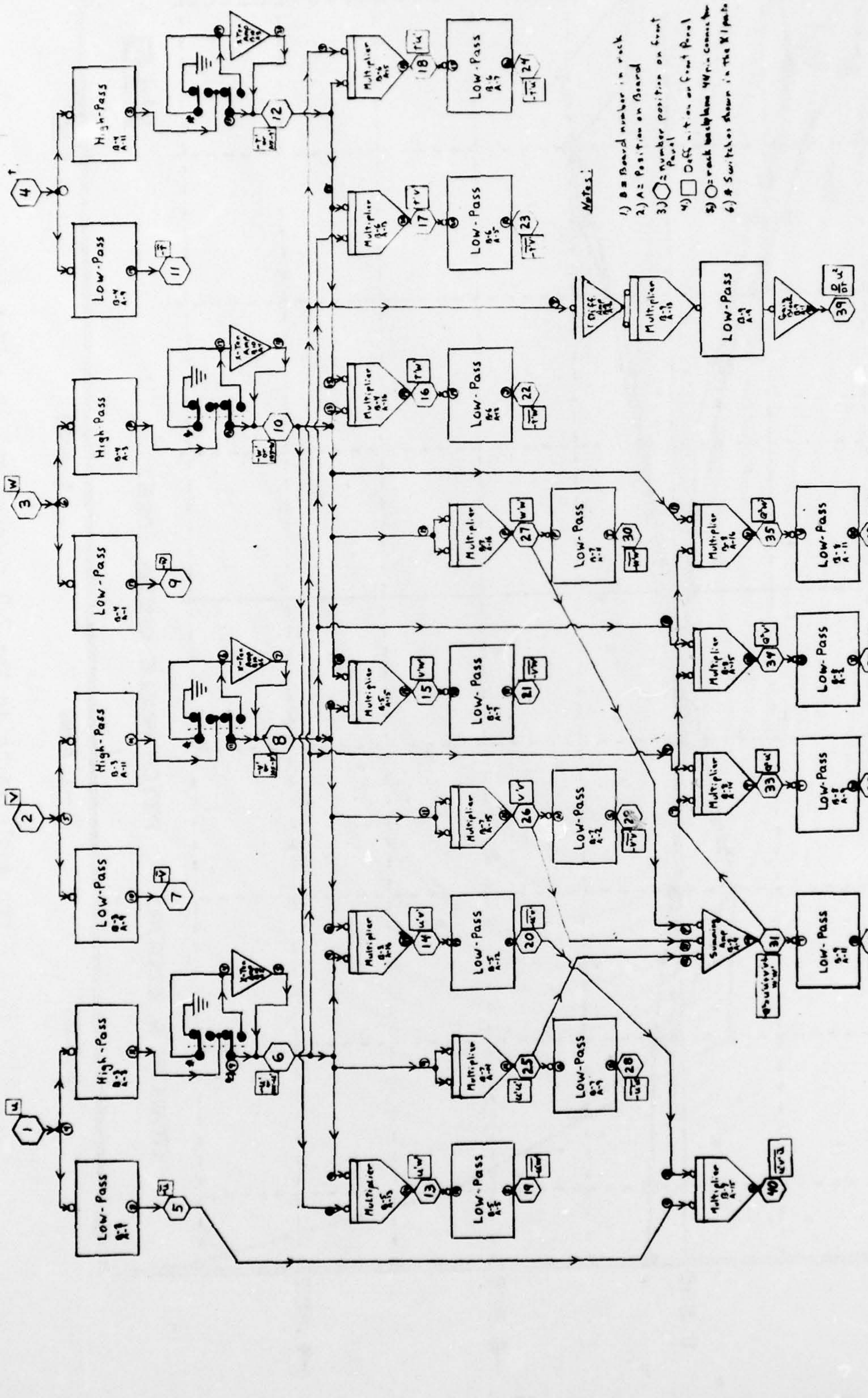

Fig. 25. Schematic of the Post Processor.

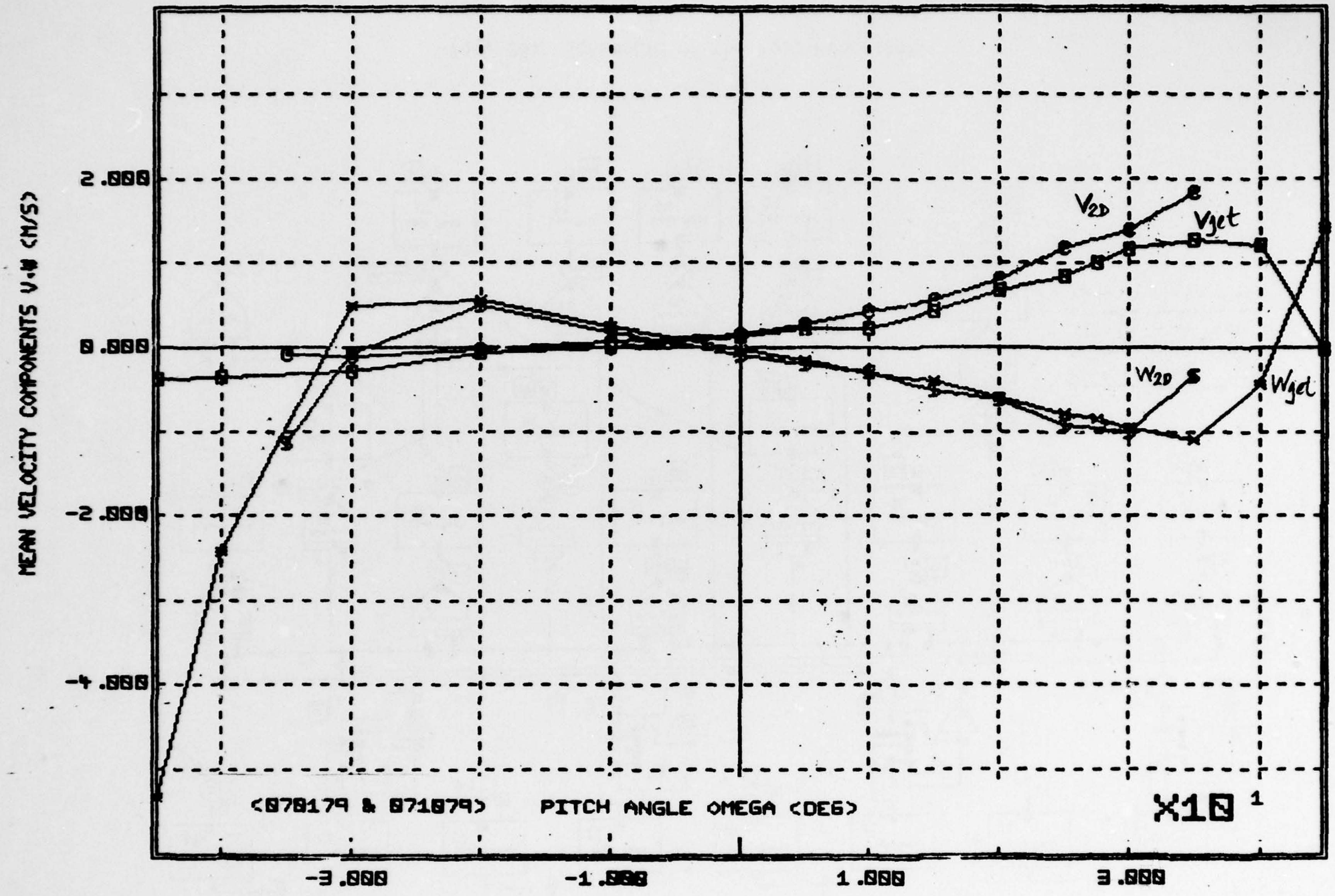

Fig. 26. Pitch angle tests in the 2-D channel and in a free jet.

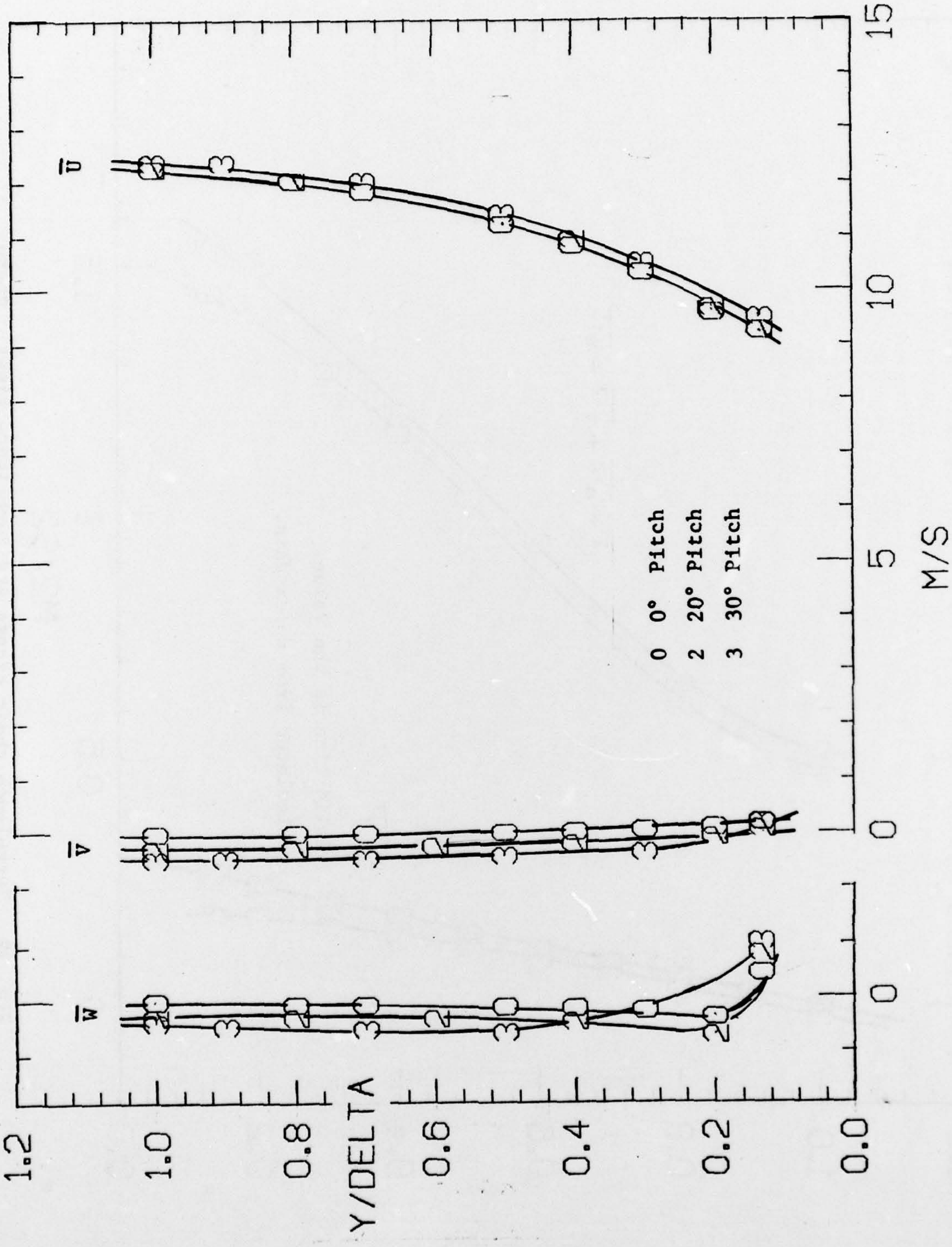

Fig. 27. Mean velocity measurements at 0° and 20° pitch.

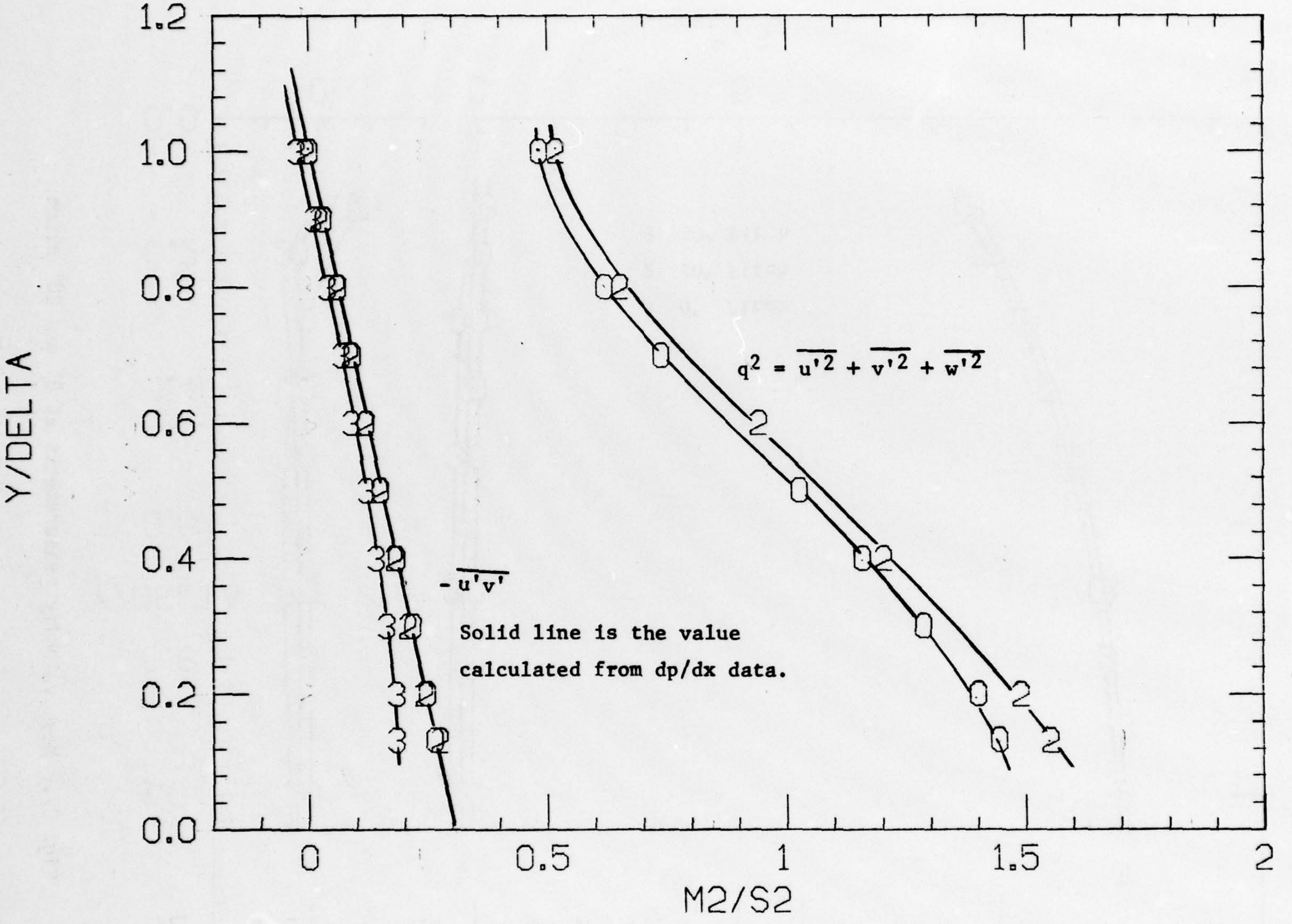

Fig. 28. Turbulence shear stress and turbulence kinetic energy, at 0 and 20 degrees pitch.

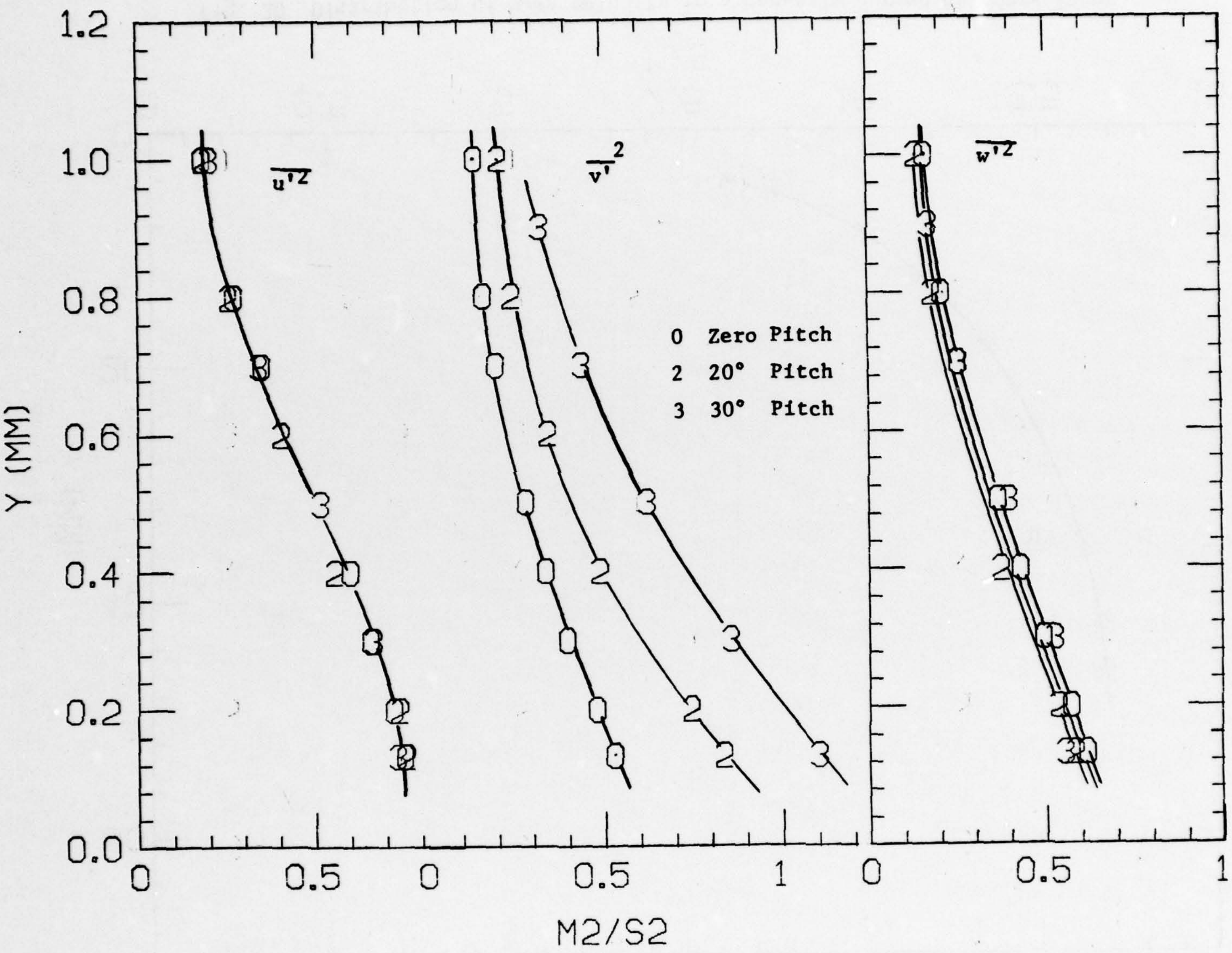

Fig. 29. Turbulence components $\overline{u'^2}$, $\overline{v'^2}$, and $\overline{w'^2}$ at 0° and 20° pitch.

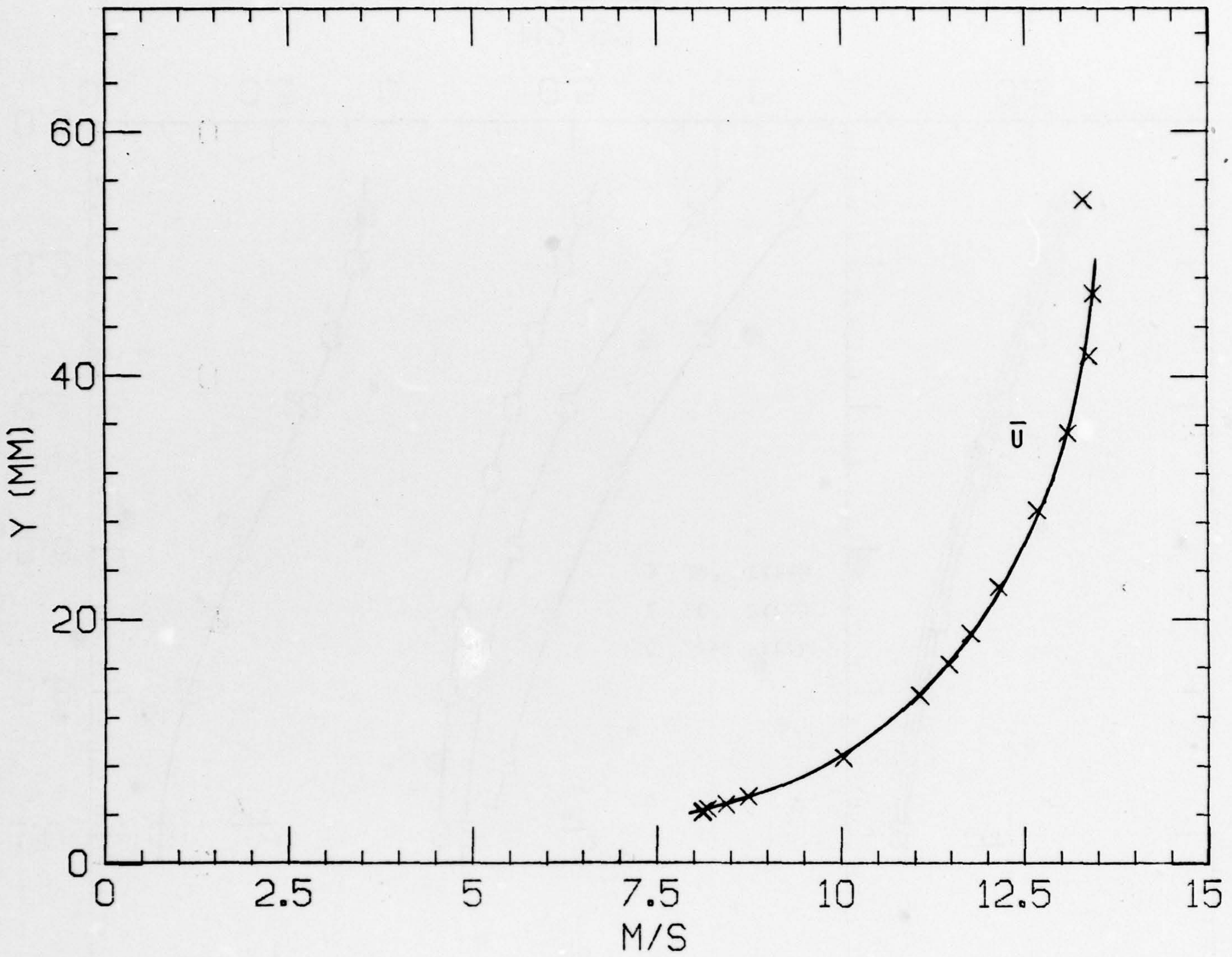

Fig. 30 Distribution of mean velocity in a convexly curved boundary layer

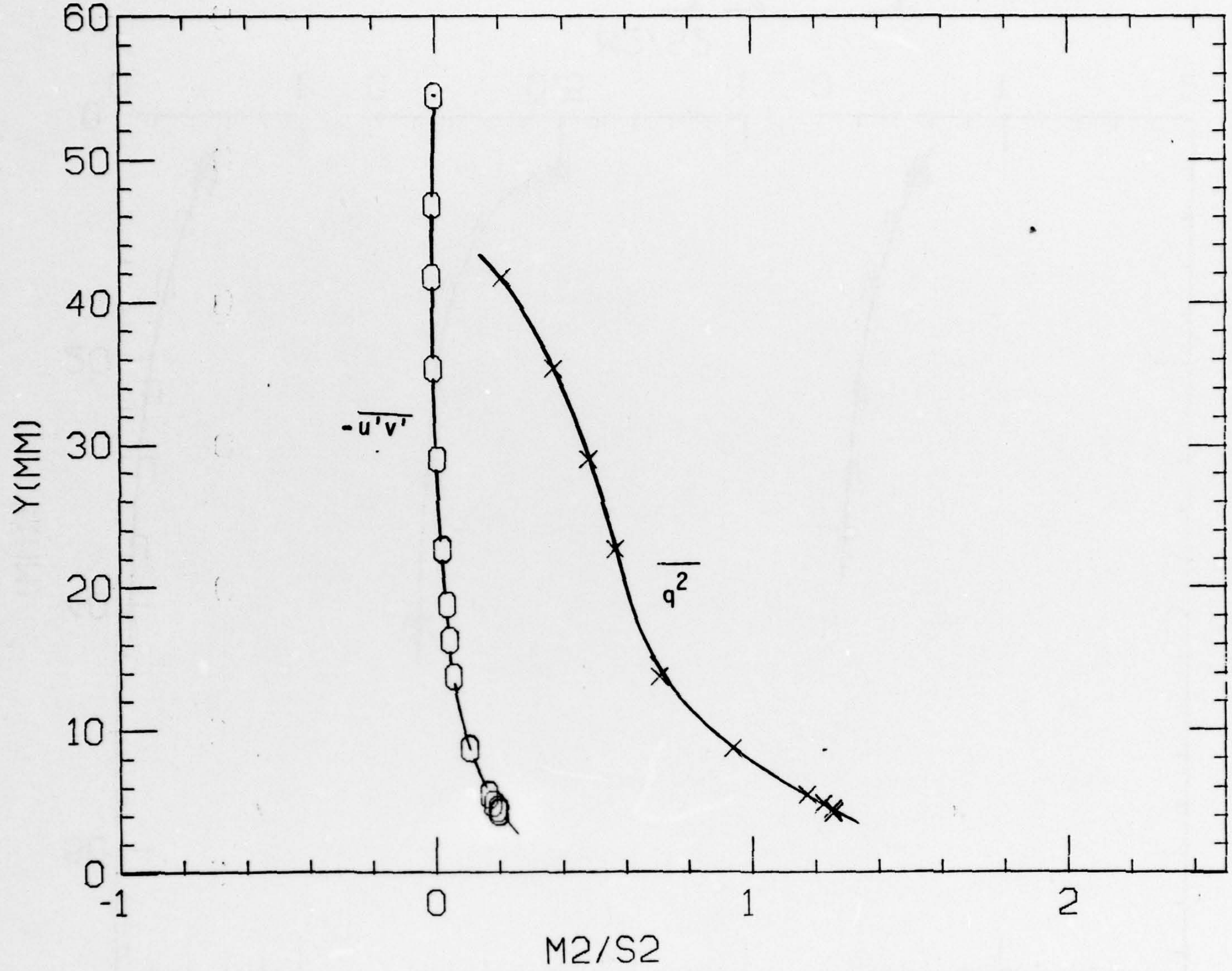

Fig. 31. Turbulence shear stress and kinetic energy distributions, $-\overline{u'v'}$ and $\overline{q^2}$ in a convexly curved boundary layer.

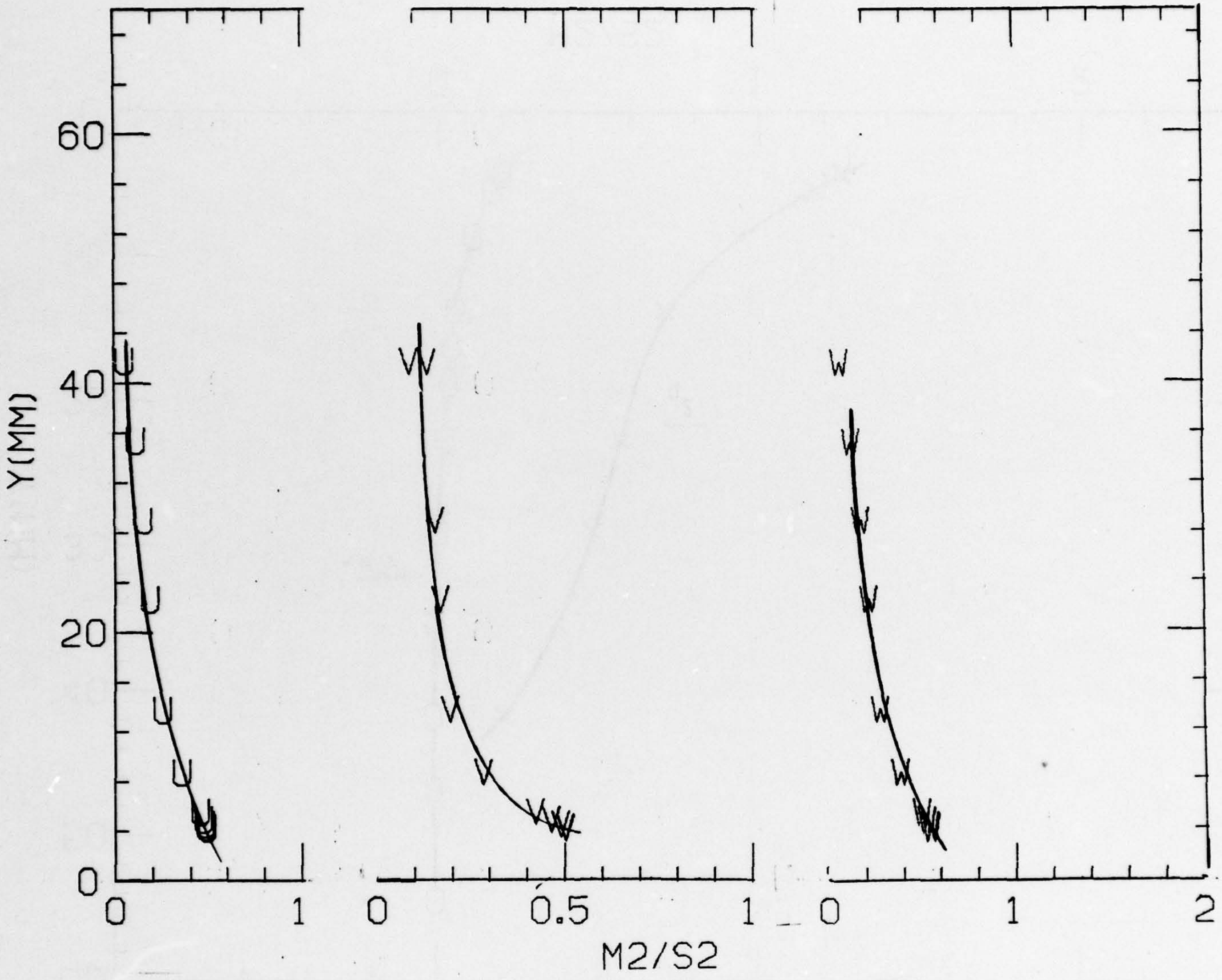

Fig. 32. Turbulence components $\overline{u'^2}$, $\overline{v'^2}$, and $\overline{w'^2}$ in a convexly curved boundary layer.

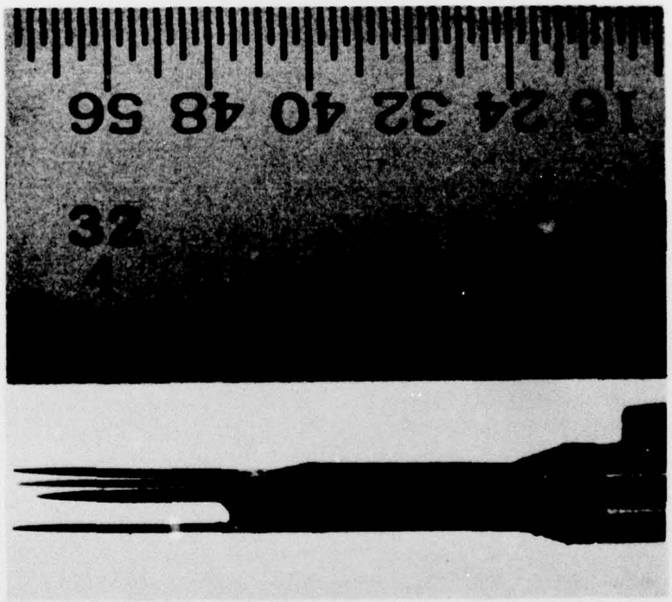

Figure 33 The miniature triple wire probe, Design #1